Effect of calcium stearate on cellulose acetate-based mortars

Joe Tannous, Thouraya Salem, Othman Omikrine Metalssi, Teddy Fen-Chong

Effect of calcium stearate on cellulose acetate-based mortars

Joe Tannous[a,*,b], Thouraya Salem[b,1], Othman Omikrine Metalssi[b], Teddy Fen-Chong[b]

[a]*ESITC-Paris,79 Av. Aristide Briand, Arcueil 94110, France*
[b]*Univ Gustave Eiffel, Cerema, UMR MCD, Marne-la-Vallée F-77454, France*

Highlights

- CA and CS addition increases the porosity and modifies the pore size distribution.
- 1 wt% CS by weight of cement leads to better hydration of the CA-based mortars.
- CS addition reduces the amount of interconnected capillary pores.
- 1 wt% CS reduces the shrinkage of CA-based mortars.
- 10_MK_SP achieves optimal workability, shrinkage and mechanical performance.

Abstract

The purpose of this study is to investigate the properties of cellulose acetate-based mortars with the addition of calcium stearate (CS), superplasticizer (SP) and metakaolin (MK). Previous research has shown that cellulose acetate (CA) fibers from industrial cigarette butts (CB) treatment can be incorporated into standard mortars at a rate of 1.3 wt%. CS was added in various proportions by weight (0.5, 1, 1.5 wt%), and their influence on cement hydration and microstructure was studied using various investigative techniques. The addition of CS was found to be beneficial in reducing the amount of water absorbed by CA, despite the significant absorption of these fibers. Furthermore, a CS rate of 1 wt% decreased CA-based mortar shrinkage. Additionally, 1 wt% CS improved by 18% the compressive strength of CA-based mortars manufactured with SP compared to the reference CA-mortar. CA fibers and CS seem to modify mortar microstructure by creating a plurimodal pore size distribution and reducing capillary pores. The CS addition, however, resulted in more cracks and reduced workability due to the weakening of the bond between the cement paste components. MK-mortars showed a slight 15% reduction in compressive strength and 13% reduction in bending strength; along with a 20% increase in shrinkage. By incorporating CA fibers as an additive along with CS or MK, CA-based mortars can improve some properties, including shrinkage and mechanical strength. Further, this approach offers a potential solution to CB pollution by reducing the environmental impact of this waste.

Keywords

Mortar; damp proofing material; microstructure; biosourced materials; mechanical properties

1. Introduction

Climate change, CO_2 emissions and natural resources depletion pose significant challenges to the construction industry. The World Business Council for Sustainable Development (WBSCD)

* Corresponding author at: *Univ Gustave Eiffel, Cerema, UMR MCD, Marne-la-Vallée F-77454, France*.
E-mail address: joe.tannous@univ-eiffel.fr (J. Tannous).
[1] Present address: *Univ Gustave Eiffel, Cerema, UMR MCD, Marne-la-Vallée F-77454, France*.

reported that global temperatures have already surged by over 1°C. This significant rise is mostly attributed to the increase in CO_2 concentrations in the atmosphere [1]. Global waste production is projected to increase by 70% by 2050 if no urgent action is taken [2]. In France, nearly 240 million tonnes of waste were generated in the construction industry in 2018 [3]. Worldwide, over 40% of waste production is inadequately managed, with incineration and landfilling being the most common disposal methods [4]. The construction sector worldwide accounts for over 36% of the total energy consumption and contributes to 40% of CO_2 emissions [5]. In France, this sector consumes more than 30% of natural resources [6].

The use of alternative materials in construction has become a necessity to preserve nature and humanity. Many countries are tackling this challenge, especially France, as its construction sector consumes 43% of energy and contributes to 23% of greenhouse gas emissions [7]. Thus, this has led researchers to develop environmentally friendly and sustainable building materials. These innovations enable energy savings, waste recycling, and compliance with environmental requirements.

Numerous studies have investigated the influence of natural or recycled fibers within the cementitious matrix. Fibers have been shown to improve various properties of existing construction materials. Natural fibers and bio-based materials showed significant properties that enhance their suitability as construction materials in several aspects. These include acoustic absorption and thermal insulation [8], [9], [10], [11], [12], fire prevention [13], carbon storage [14], and tensile strength [15]. For instance, in [16], the incorporation of diss fibers in the cement matrix led to lighter composites with improved thermal insulation. With a 30% fiber content, thermal conductivity was reduced by 76% compared to the reference. Moreover, this addition enhanced composites toughness under flexion and compression, improving post-failure behavior.

Cigarette butts (CB) are an example of waste requiring recycling. Worldwide, CB are the most common litter waste found in the environment [17]. Global cigarette production was estimated at 5.7 trillion cigarettes in 2016 [18]. According to [19] cigarette production will reach 9 trillion by 2025. As for cigarette smoke, it contains more than 7 000 toxic compounds. Cigarette filters retain these substances, including approximately 4000 toxic chemicals such as nicotine [20]. However, cigarette filters can be found thrown on the ground and beaches. Due to rainfall and various weather conditions, CB are carried to drainage systems and eventually reaches the ocean [21]. One thrown cigarette can contaminate more than 1000 litres of water. Once nicotine is entirely leached into the water, its concentration can surpass the European Union limit for tobacco waste [22].

This waste threatens several ecosystems due to its toxic compounds and biodegradability resistance [22]. Cigarette filters are usually composed of 97 wt% of cellulose acetate (CA), a modified natural polymer with low biodegradability, approximately 7.5-14 years [22], [23]. In addition to the limited collection of this waste, most of it is incorrectly eliminated. Landfilling and incineration are not the most appropriate methods for handling cigarette butts. These methods are expensive, not durable and can leak contaminants into groundwater and the atmosphere [24], [25].

To strengthen international governmental policies aimed at decreasing cigarettes use [26], [27], researchers have developed different methods for recycling CB waste in recent years. These methods focus on transforming waste into recycled materials. CB has been valorised in various

fields, including building materials, biological wastewater treatment, paper production, activated carbon, and sound absorbers [24]. Encouraging results have been achieved.

In the building materials field, the study in [28] confirmed that CB addition increased concrete block ductility but decreased compressive strength. In another study [29], the authors used CB to improve clay bricks thermal and energy performance. The addition of 1 wt% of CB reduced thermal conductivity by 15% and saved energy up to 8% compared to reference bricks.

Multiple studies were conducted to explore the incorporation of CB in clay bricks, with incorporation rates ranging from 0 wt% to 10 wt% [30], [31], [32]. The authors observed a decrease in density, thermal conductivity, compressive strength, along with an increase in porosity, as the incorporation rate in clay bricks increased. Additionally, research focused on replacing coarse aggregates in stone mastic asphalt with bitumen-encapsulated cigarettes (1, 2 and 3 wt%) [33].

CB were incorporated at various rates, including 0%, 0.5%, 1%, 1.5%, 2% and 2.5% based on plaster weight in gypsum composites for building applications [34]. The optimal mechanical results were achieved with a 2.5 wt% addition. Both compressive and bending strengths presented a gradual increase compared to the reference. Although no significant difference was observed in acoustic absorption, these compounds can be applied in various construction applications that require good mechanical strength.

Only few recent studies have been published on the incorporation of recycled CA into concrete, mortars or geopolymers demonstrating the originality of this work.

In [35], encapsulated cellulose acetate microfibers were incorporated at various rates (ranging from 0 to 1.5%) in geopolymer mixes. The addition of CA fibers to the mixes resulted in a gradual reduction in mix workability. This reduction was attributed to the porous texture, rough surface, low density, and hydrophilic nature of CA microfibers. Furthermore, the incorporation of 1.5 wt% of CA led to a significant decrease in compressive strength, approximately 41% lower than the reference. This reduction was associated with pore formation and CA agglomeration. Moreover, the flexural strength increased by up to 4% with 0.8 wt% content. Additionally, a decrease in density and an increase in porosity and water absorption were noted. As a result, the addition of CA contributed to enhancing geopolymers thermal insulation.

Another study [36] investigated the mechanical and durability performance of different concrete mixes with CA. Different volume fractions of CA (0.5%, 1%, 1.5%, and 2.5%) were incorporated into recycled concrete mixes with recycled coarse and fine aggregates (RCA & RFA). The optimal CA rate was 1.5% for all mechanical performances. An increase in the CA rate in RCA or RFA led to a decrease in concrete's short-term durability, as indicated by increased sorptivity, porosity, and chloride penetration.

This paper presents a sequel to the previous original work regarding the potential valorisation of industrially pre-depolluted CA fibers in cementitious mortars [37]. The CA used is a product of MéGO! Company. While CA fibers have been previously used as a partial sand replacement in cementitious mortars, in this study, they are used as reinforcement at a rate of 1.3 wt% of sand.

In the preliminary study, the current authors found that CA fibers had significant water absorption. To address this issue and reduce CA water absorption, a literature review was conducted on water-repellent materials applicable to cementitious materials. It was found that calcium stearate (CS), a damp proofing material, is used as an additive in slag, mortars, concrete

and geopolymers. CS is inexpensive hydrophobic material, is derived from stearic acid, a fatty acid generally considered safe, so does not emit harmful substances [38], [39], [40]. According to [41], CS decreased water absorption, decreased pore connectivity by reducing microstructure defects, and changed the pore size distribution by forming a hydrophobic film. In this research, a 4% rate is recommended for slag. When using CS in concrete mixes, the authors of [42] noticed a 42% reduction in free shrinkage for various water/cement ratios, along with a decrease in workability and compressive strength. In another study [43], several mortars were manufactured with different hydrophobic compounds as admixtures. The authors used a water/cement ratio of 0.8 and a water-repellent admixture content of 1 wt% of cement. The CS mortars had mechanical properties very close to those of the reference mortar. CS appeared to be a suitable, inexpensive damp-proofing material with water-repellent properties.
Therefore, in this study, CS has been added by mixing it manually with CA at the rates of 0.5, 1 and 1.5 wt% of cement. CA could be hydrophobized after being coated with CS.

Furthermore, in [37], the addition of CA fibers to the mortar composition showed a negative effect on compressive strength, with the latter decreasing by 22% when 1.3 wt% of sand was replaced by CA. Metakaolin (MK) can address this issue. MK has been widely used in mortar and concrete formulations as a filler or pozzolanic material. It has been found that MK can enhance durability, mechanical properties, and improve pore structure [44], [45], [46], [47]. For instance, in [44], cement is substituted with MK within the range of 5% to 20%. It is observed that metakaolin has no significant impact on shrinkage. Also, it is assumed that the pozzolanic reaction may modify pore dimensions while maintaining constant total water absorption. The optimal MK addition is between 10% and 15%. When incorporating metakaolin at a 10% rate, along with 10% silica fume and 6% coconut fibers, the authors in [48] achieved significantly improved mechanical and physical properties in the studied mortars. In comparison to the reference mix, the optimal formulation resulted in a 28.3% increase in compressive strength at 28 days.

This paper aims to investigate the effects of CS at rates of 0.5, 1 and 1.5 wt%, as well as MK at a rate of 10 wt% (following [44], [45], [46], [47], [48]), on the macroscopic and microscopic properties of mortars with the addition of 1.3 wt% of CA. The purpose of including three different CS rates is to determine the most effective rate for ensuring optimal coverage of CA fibers, and evaluate their impact on CA-based mortars. The selection of 1.3% CA follows previous research where it was identified as the optimal rate. These additives were introduced into mortars with and without a superplasticizer (SP) at a rate of 3%. This rate was also determined in the earlier study by the authors, based on workability results of the CA-based mortars.
Thermogravimetric (TGA), mercury intrusion porosimeter (MIP) and scanning electron microscope (SEM) analyses were conducted to identify the effects of these additions on the paste and the hydration process, as well as to characterize pore size and distribution. The microscopic results were correlated with the test results of fresh mortars (workability) and hardened mortars, including shrinkage, mechanical strength and density. The results of this research could contribute to reducing the harmful ecological impact of discarded cigarette butts.

2. Materials and methods

2.1 As-received materials

2.1.1 Sand, cement, superplasticizer

The materials used in this study are those described in the preceding article by the authors. These materials include:

- Sand: Standard sand in accordance with CEN EN 196-1 [49], ISO 679 [50], sourced from 'Societe nouvelle du littoral'. The sand characteristics are cited in **Table 1**, and its particle size distribution is presented in **Fig. 1**.

Table 1. Sand properties.

Apparent density (kg/m^3)	2640
Bulk density (kg/m^3)	1620
Fineness modulus	2.6 – 2.7
Loss on ignition (LOI) at 950°C	0.16
Water absorption (%)	0.20
Al_2O_3 (%)	0.25
Fe_2O_3 (%)	0.06
P_2O_5 (%)	0.00
TiO_2 (%)	0.02
SiO_2 (%)	98.69

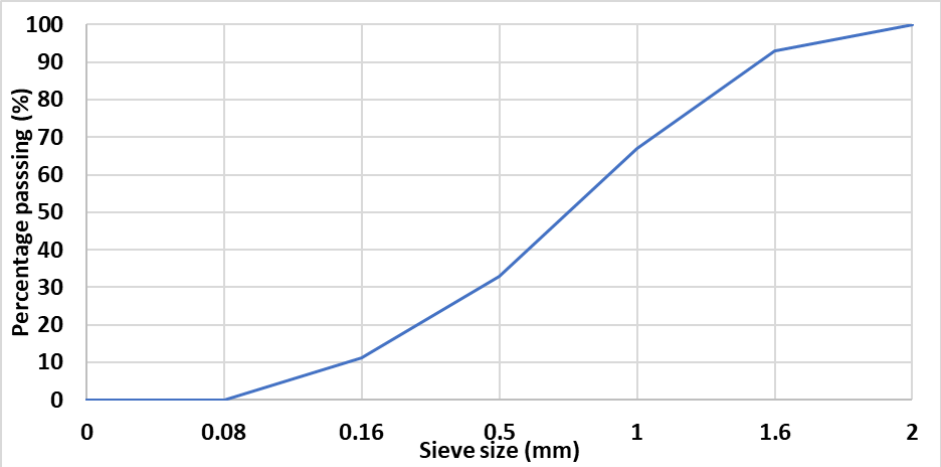

Fig. 1 Particle size distribution of the used sand.

- Cement: CEM I 52.5 N CE CP2 NF in accordance with NF EN 196-1 [49]. The sand-to-cement ratio is established at 3. The cement's composition, as provided by the manufacturer is detailed in **Table 2** (note that this was inaccurately stated in [37]). The compound composition was determined using the Bogue equation, as shown in **Table 3**.

Table 2. Cement composition.

Components	**wt (%)**
CaO	62.79
SiO_2	20.38
AL_2O_3	4.30
Fe_2O_3	3.80
MgO	1.25

SO_3	3.46
S	Traces
K_2O	0.73
Na_2O	0.35
Chlorides	0.04
MnO	0.05
LOI (loss on ignition)	2.04
Insoluble	0.54
∑	99.97
Free lime	1.39
LSF (Lime saturation factor)	0.97
SR (Silica ratio)	2.51
AR (Alumina ratio)	1.13

Table 3. Anhydrous cement composition calculated by Bogue method based on the information given in Table 2.

Components	Mass content based on Bogue equation (%)
C_3S	57.05
C_2S	14.99
C_3A	7.91
C_4AF	8.9

- Superplasticizer (SP): SikaViscoCrete Tempo 653 superplasticizer in accordance with EN 934-2 was employed. SP is specifically designed to improve mixtures workability.

2.1.2 CA fibers

CA fibers, illustrated in (**Fig. 2**), are a product of MéGO! Company, which employs a partially autonomous depollution process to recycle CB. According to the supplier, the current annual availability of CA fibers for MéGO! company is 20 tons, with a progressively increasing quantity each year.

Upon collection of the butts, the used filters undergo careful sorting to eliminate all unwanted waste. At this stage, the tobacco is separated for composting. The company imposes strict protocols to ensure the efficiency of the sorting process. Following this step, the butts are ground and then depolluted using a washing technique in which the main solvent is rainwater, without the addition of any chemicals. The water is then recycled in a closed circuit. This phase guarantees the cleaning of the butts and the removal of harmful substances. Finally, the fibers are dried and ground once more.

The studied CA fibers have been examined by several tests to determine their environmental impact. First, CB, which contain polar molecules, were treated with water. Water, being a polar solvent, is used to remove contaminants from the cigarette butts. This pre-treatment

step likely aids in separating unwanted substances from the butts, making them more suitable for recycling.

Then the CA obtained after this process were tested by SGS (Société Générale de Surveillance) to ensure that they comply with quality, safety, health, and environmental regulations. The performed tests include SVHC (Substances of Very High Concern) and Annex XVII both identified under the European Union's REACH (Registration, Evaluation, Authorisation, and Restriction of Chemicals) regulation, and POP (Persistent Organic Pollutants) regulations.

The reports have shown that i) the tested SVHC levels, ii) the organotins, cadmium and PAH (Polycyclic Aromatic Hydrocarbons) quantities as per Annex XVII regulations, and iii) the results of POP tests all remain within acceptable limits, not exceeding the established guidelines. Using ICP-AES method, complementary mineralogical analysis was conducted on CA leaches indicating non-significant percentages for Al, Fe, Mn, P, and Ti, with low percentages of Mg, Si, Ca, K, and Na.

The fibers were dried at 60°C until mass variation less than 0.1% over 24 h, following the recommendation of RILEM TC-236 BBBM [51], to determine their physical parameters. These parameters include:

i) Bulk density, both without and with compaction, measuring 39 ± 3 kg/m^3 and 65 ± 2 kg/m^3, respectively;

ii) Total porosity, which stands at 97 ± 1%;

iii) Water absorption after 1 minute of immersion (IRA), recorded at 500 ± 146%.

Additional information regarding the fiber properties can be found in [37] as the same batch have been used. It is noted that the supplier has indicated that batches may vary depending on the flows of cigarettes received and the fact that the material is not homogeneous.

Several studies have been conducted on two different batches of fibers with a one-year difference between their reception, assessing their properties through density, FTIR, TGA, water absorption, initial water content tests, and SEM observations. The findings indicate that their properties are similar.

The cost of CA fibers is low since they are generated from waste collected from MéGO! clients. The primary cost is associated with the depollution process of the fibers within the closed circuit.

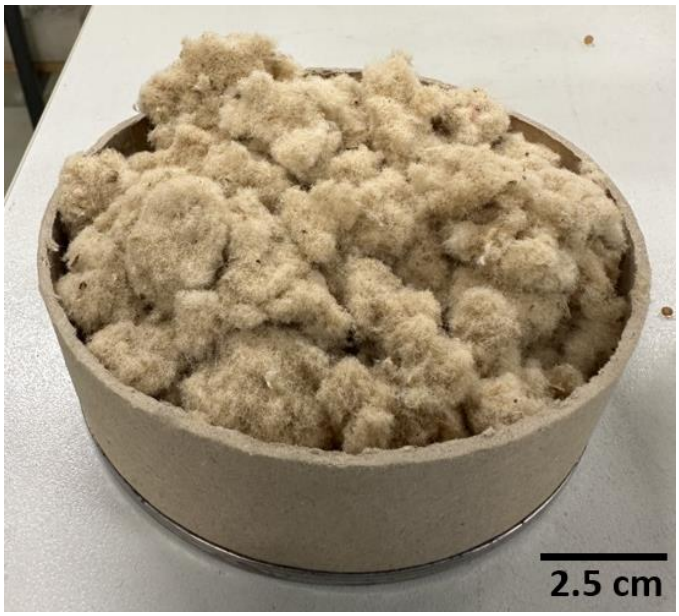

Fig. 2. Cellulose acetate (CA) fibers as provided.

2.1.3. CS powder

Calcium stearate (CS) is a white, water-insoluble powder, as shown in **Fig. 3a**. It is a product from the Thermo Fisher Scientific brand. It has a molecular weight of 607.03 g/mol. CS particles exhibit an irregular, plate-like shape with angular edges. **Table 4** summarizes the essential physical and chemical properties of CS, while **Fig. 3b** displays a scanning electron microscopy image of this material.

Table 4. Physical and chemical properties of calcium stearate.

Appearance	White to off-white powder
Solubility	Water insoluble
Melting point (°C)	145 – 160
Stocking temperature	Room temperature
Chemical formula	$C_{36}H_{70}CaO_4$
Molar mass (g/mol)	607.03
Titration complexometric (%)	6.4 to 7.5 (Ca)
Loss on drying (%)	≤ 6 (105 °C, 3 hrs)
Ash (%)	9 % to 10.5

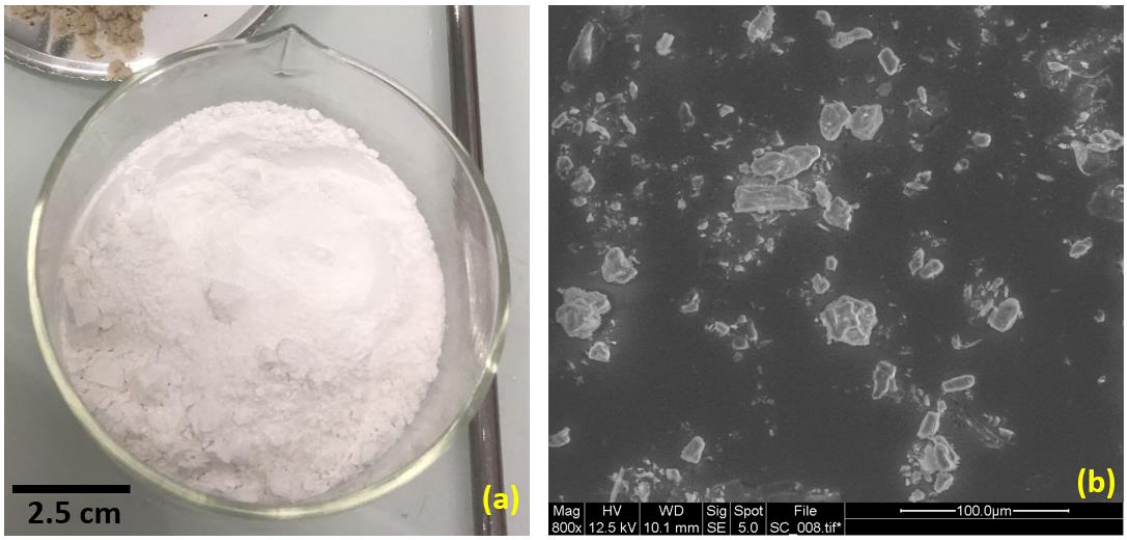

Fig. 3. Calcium stearate (CS): (a) Physical aspect, (b) SEM.

2.1.4. Metakaolin

The metakaolin (MK) used is a high-reactivity metakaolin pozzolan known as 'Metamax'. It is produced through the thermal activation of high-purity Kaolin clay within a specific temperature range. It is manufactured by 'BASF Corporation Company, USA'. Its composition is in accordance with '2012 OSHA Hazard Communication Standard; 29 CFR Part 1910.1200' regulation. **Table 5** presents the physical and chemical properties of the metakaolin used.

Table 5. Physical and chemical properties of metakaolin

Melting point (°C)	1300
Solubility in water	Insoluble
Free moisture (%)	0.5
pH	6
Median particle size (µm)	1.3
Specific gravity (g/cm^3)	2.50
Bulk density (kg/m^3)	320

2.2 Sample preparation and manufacturing

After conducting preliminary tests using CA fibers as a sand replacement, the initial study by the present authors [37] determined the optimal rate of 1.3 wt% of CA with 3 wt% of SP.
In this paper, CA fibers are used as an addition at the same rate as previously determined, of 1.3 wt% of sand. At this rate, no fiber agglomeration is observed. Also, CA was added to investigate its potential in reinforcing the mortar and reducing its shrinkage without having a significant impact on the microstructure.
SP was employed at a rate of 3 wt% of cement. The water/cement ratio was fixed at 0.5. CS was added at different rates: 0.5, 1 and 1.5 wt% of cement. These three rates were selected to identify

the optimal addition rate. Additionally, a mixture was studied using 10% by weight of cement of MK as an additive, following [44], [45], [46], [47], [48].

It is important to mention that SP rate was fixed according to the authors' preliminary work, and it remained constant across all formulation without considering the consistency of the mixes. The main goal was to examine the influence of CA fibers and other additives on mortar properties, with a fixed water/cement ratio in all mixes, thus avoiding the introduction of another new variable. The studied formulations are presented in **Table 6**.

Table 6. The studied formulations.

Description	N°	Designation	Components
I – References	1	Rf_0	Sand (S), Cement (C), Water (W)
	2	Rf_0_SP	S, C, W, 3 % SP
	3	Rf	S, C, W, 1.3 % CA
	4	Rf_SP	S, C, W, 1.3 % CA, 3 % SP
II – Mixes with CS, without SP	5	0.5_CS	S, C, W, 1.3 % CA, 0.5 % CS
	6	1_CS	S, C, W, 1.3 % CA, 1 % CS
	7	1.5_CS	S, C, W, 1.3 % CA, 1.5 % CS
III – Mixes with CS, with SP	8	0.5_CS_SP	S, C, W, 1.3 % CA, 0.5 % CS, 3 % SP
	9	1_CS_SP	S, C, W, 1.3 % CA, 1 % CS, 3 % SP
	10	1.5_CS_SP	S, C, W, 1.3 % CA, 1.5 % CS, 3 % SP
IV – Mix with MK	11	10_MK_SP	S, C, W, 1.3 % CA, 3 % SP, 10% MK

First, and independently from the mix, CS was manually mixed with CA fibers for 2 minutes (**Fig. 4).** This process enables the coating of fibers with CS, resulting in a reduction of CA water absorption. SEM observations were conducted on 1.3 wt% CA covered with 1 wt% CS. **Fig. 5** illustrates that CS can adhere to the fiber surfaces and coat a significant portion of them, yet it incompletely covers the totality of CA.

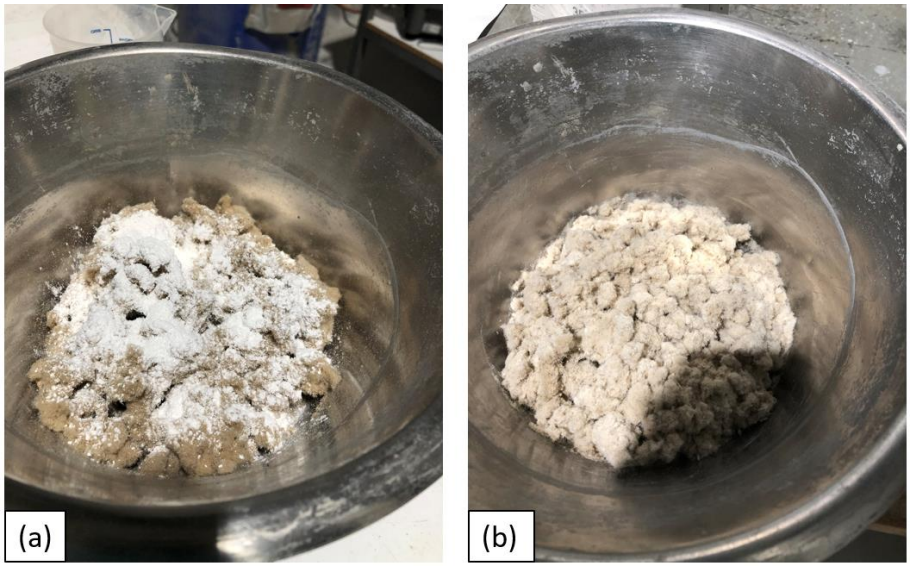

Fig. 4 CA and CS (a) before mixing and (b) after mixing.

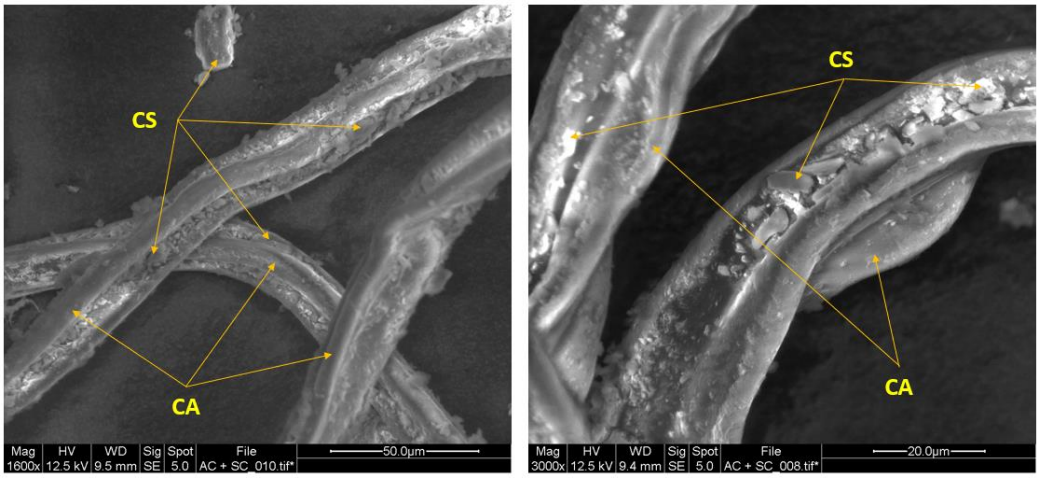

Fig. 5 SEM of 1.3 wt% CA coated with 1 wt% CS.

A specified mortar mixing protocol was established based on the literature review, preliminary tests and workability results. At first, cement, water and sand are mixed at low speed (100 rpm) in the mixer for 1 minute. Afterward, the mortar is removed from the bowl surface and gathered in the center for about 30 seconds. If the formulation includes superplasticiser (SP), it is added at this point. Next, CA fibers coated with CS, prepared beforehand, are gradually introduced into the mixer for 20 seconds to prevent mass loss of CA and CS, given their volatile nature. Then, all components are mixed together for 1 minute at high speed (300 rpm), and the mortar is scraped from the bowl surface. Finally, the mortar undergoes an additional 1 minute mixing at high speed (300 rpm). The resulting mixture is used to produce 4x4x16 cm^3 samples as shown in **Fig. 6a** . For the mechanical and microstructural tests, the specimens were stored in a temperature-controlled water tank at a fixed temperature of 20 °C after demolding (**Fig. 6b**).

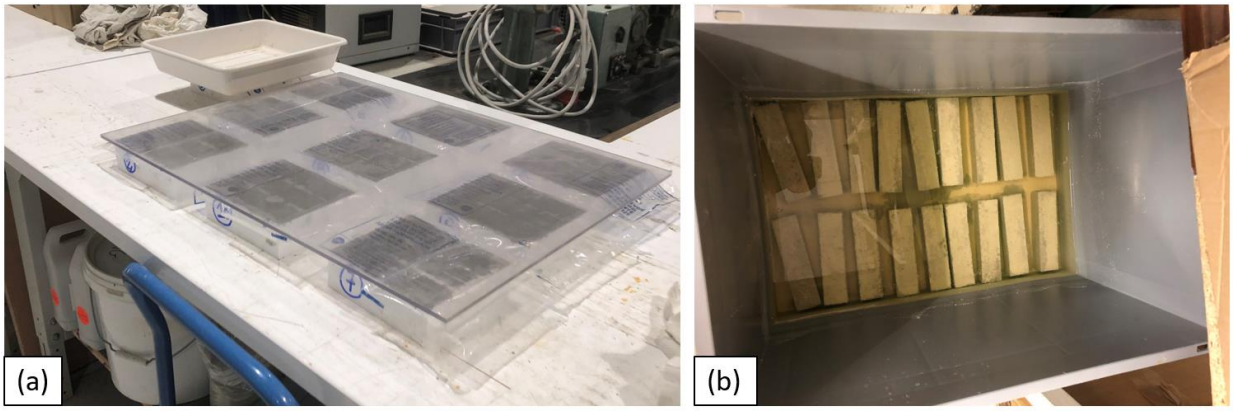

Fig. 6 The studied CA-based mortars (a) after manufacturing and (b) stored in a water tank.

2.3 Experimental methods of characterization

2.3.1 Microstructural characterization

After crushing the mortars, the samples are dried at 60°C until their relative mass variation is less than 0.05% then sieved at 315 µm. Thermogravimetric analyses (TGA) are then conducted on the particles passing the sieve to determine the chemical composition of the mortars.

TGA is a thermal analysis plotting mass variation against temperature. This analysis was performed using the Netzsch STA 449 Fx Jupiter® analyser under a nitrogen atmosphere to maintain inert conditions. The recorded data include i) the temperature range from 25 to 1250°C, ii) a heating rate of 10 k/ min, and iii) information regarding sample mass loss.

The derivative DTG enables the identification of specific temperature values associated with significant mass losses.

The materials and the mortar's microstructure were examined through a series of tests, including Microstructural Porosity by Mercury Injection (MIP) and Scanning Electron Microscope (SEM) analysis.

Mercury Intrusion Porosimetry (MIP) is employed to determine the pore size distribution and open porosity of the samples. The Micrometrics Autopore IV 9520 Porosimeter serves as the testing device for this purpose. The MIP test includes two phases. At first, air is evacuated from the penetrometer, allowing mercury to fill it under a small pressure of 0.1 MPa. Then, pressure is gradually increased to allow mercury infiltration into smaller pores. The second phase consists of immersing the sample in a hydraulic fluid under high pressure, approximately 414 MPa.

A scanning Electron Microscope (SEM) observations are conducted on CS, CA coated with CS and the mortar samples. The FEI Quanta 400 scanning electron microscope is utilized in the SE mode. These observations are qualitative and help illustrating the microstructural morphology of the tested samples.

2.3.2 Macrostructural characterization

The workability test is performed using Abrams cone, according to NF EN 12350-2 [52]. In this test, fresh mortar is poured into the cone in three layers, with each layer corresponding to approximately one-third of the cone's height. Each layer is compacted with 25 uniformly distributed strokes across the cross-section, using a compacting rod. The top layer's surface is leveled by rolling the compacting rod over it. After removing the cone vertically, the slump is determined by calculating the difference between the cone's height and that of the highest point of the specimen.

To determine shrinkage, samples are subjected to controlled conditions according to NF P 15-433 [53], with a relative humidity of 50% and a temperature of 20 °C. These conditions allow control of the main factors influencing shrinkage. During this test, mortar length is measured over time using a Mitutoyo-Controlab micrometer. The mass variation of the samples is also monitored over time.

The mechanical properties of the mortars are established at 28 days according to NF EN 196-1 [49] through three-point bending and compression tests. The tests are conducted using a Controls Pilot4 hydraulic press, with load rates set at 50 N/s for bending and 2400 N/s for compression.

Three different samples were tested for each formulation, and for each of them, a standard deviation was calculated.

The WAPT test is conducted according to the standard method NF P18-459 [54]. This method is detailed in [55], [56]. Generally, WAPT consists of two stages:

i) Air removal from the pores is achieved through partial vacuum (at 30 mbar) for 1 hour;
ii) Under the 30 mbar of vacuum pressure, water is introduced to the containers holding the samples for 44 h. This process forces water to penetrate the connected pores with diameters larger than 100 nm.

Afterward, the samples are dried at 60°C until their relative mass variation is less than 0.05%. Importantly, this temperature does not impact the microstructure [56].

The dry density of mortars is determined by dividing the mortar mass by its volume. This evaluation was conducted at 28 days, using a calliper with 0.01 mm precision to measure dimensions and a scale accurate to 0.01 g.

3. Results and discussion

3.1. Microstructural properties

3.1.1 Thermogravimetric analysis (TGA)

Thermogravimetric tests were conducted on the mortars at 28 days, focusing on the core part of the mortar. In **Fig. 7 (a-b),** the mass losses of different phases in the TGA curves and their derivative (DTG) are represented. The peak occurring between 30 and 200 °C represents the decomposition of C–S–H, ettringite, and mostly the loss of free-water [57]. Just below 200 °C, a peak confirms the presence of monosulfoaluminates (AFm). The peak in the range of 450 and 550 °C corresponds to the dihydroxylation of Portlandite: $Ca(OH)_2$ [58]. The third peak, between 650 and 820 °C, stands for the decarbonization of calcite $CaCO_3$.

In the mixes without SP (**Table 7** & **Fig. 7a**), the reference mortar without CA (Rf_0) exhibits the lowest amount of free water at 3.87%, while the reference with CA (Rf) has the highest free water content at 9.02%. This can be explained by the presence of CA in the mix, which will lead, over time, to the release of a significant amount of free water absorbed by CA during manufacturing.

An increase in the CS content from 0.5%, to 1%, to 1.5%, results in gradual decreases in the peaks of free water, ettringite and C–S–H, reducing from 5.17%, to 4.95%, to 4.85%.

When comparing the mass variation of free water between the mixes without SP and its equivalent with SP, it is noticed that the addition of SP has a notable effect on the quantity of free water, as shown in (**Table 7**), and in **Fig. 7a** (without SP) and **Fig. 7b** (with SP). The addition of SP generally reduces the amount of free water; except for 0.5 CS, it increased from 5.17% to 5.85%. The mass variation of free water is 9.02% for the reference mortar without SP (Rf). In contrast, for the reference with SP (Rf_SP), the mass variation equals 6.6%. This observation aligns with the findings in [59]. The authors in [60] explained that the presence of a SP improves the dispersion of cement particles, leading to better hydration and, consequently reducing the amount of free water.

In the mixes with both SP and CS (**Table 7** & **Fig. 7b**), the mix 1_CS_SP shows the lowest peak of free water at 4.32%. This result shows that a CS content of 1% optimally covers a significant

portion of the fibers, reducing water absorption by CA. These findings indicate that fibers continue to absorb water during mortar fabrication, even with a CS coating. However, the amount of absorbed water is lower than in mixes without CS but with CA (Rf and Rf_SP). A study [61] demonstrated that CS addition reduces free water content, possibly because stearate groups react with C–S–H, forming a lighter, wax-like compound compared to C–S–H particles [59].

The mass loss of Portlandite $Ca(OH)_2$ increases from 1.32% for the reference (Rf_0) to 1.75% and 1.77% respectively, for the CA reference mixes without (**Fig. 7a**) and with SP (**Fig. 7b**).

The difference in mass variation of Portlandite $Ca(OH)_2$ indicates that CA fibers enhance cement hydration. This improvement can be attributed to water release from CA fibers [37].

However, when CS is added, CA fibers effect on improving hydration decreases. As shown in (**Table 7** & **Fig. 7 (a-b)**), Portlandite mass variation decreases below 1.75% for mixes without SP (Rf) and 1.77% for mixes with SP (Rf_SP). This decrease is due to CS hydrophobic character, which decreases water absorption by CA fibers. After the addition of CS, and according to Portlandite mass variation , the optimal values are as follows: for the mixes without SP, 1.69% for 1_CS, and for the mixes with SP, 1.77% for 0.5_CS_SP.

The lowest value is observed in the mix with metakaolin equal at 0.96%. This decrease in mass loss is attributed to the consumption of produced portlandite by metakaolin over time [62]. When kaolin is heated to a temperature between 650 – 900 °C, a percentage of its mass is lost as bound hydroxyl ions (OH^-) [63]. At this temperature, the kaolin structure, composed of alumina and silica layers, is destroyed, creating a highly chemically reactive phase [64].

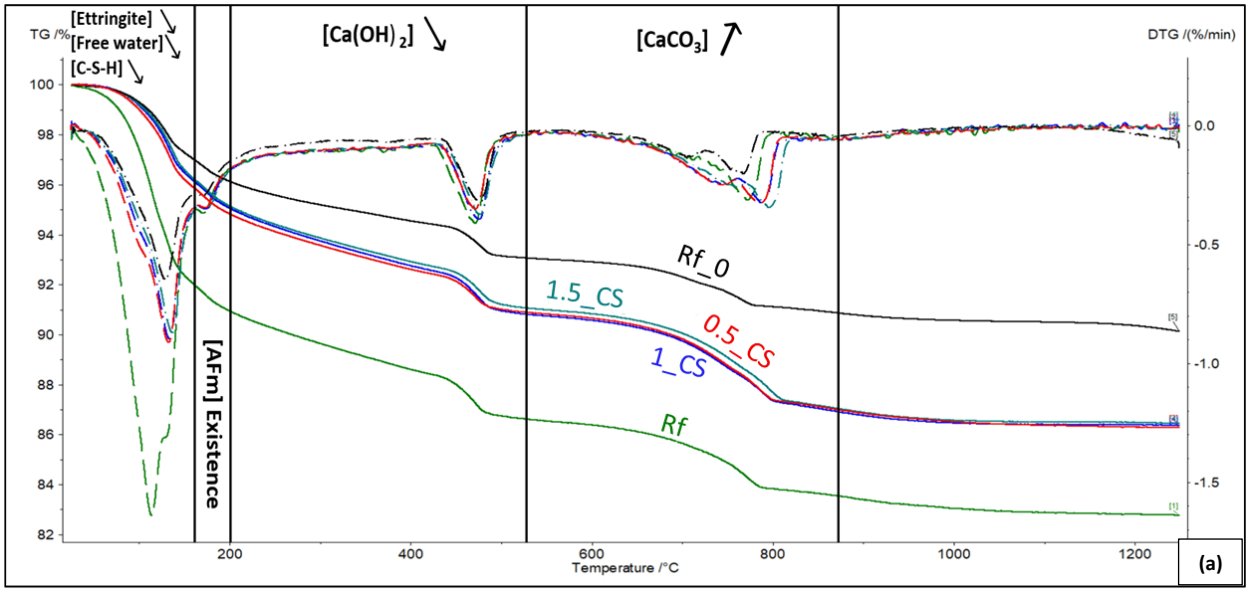

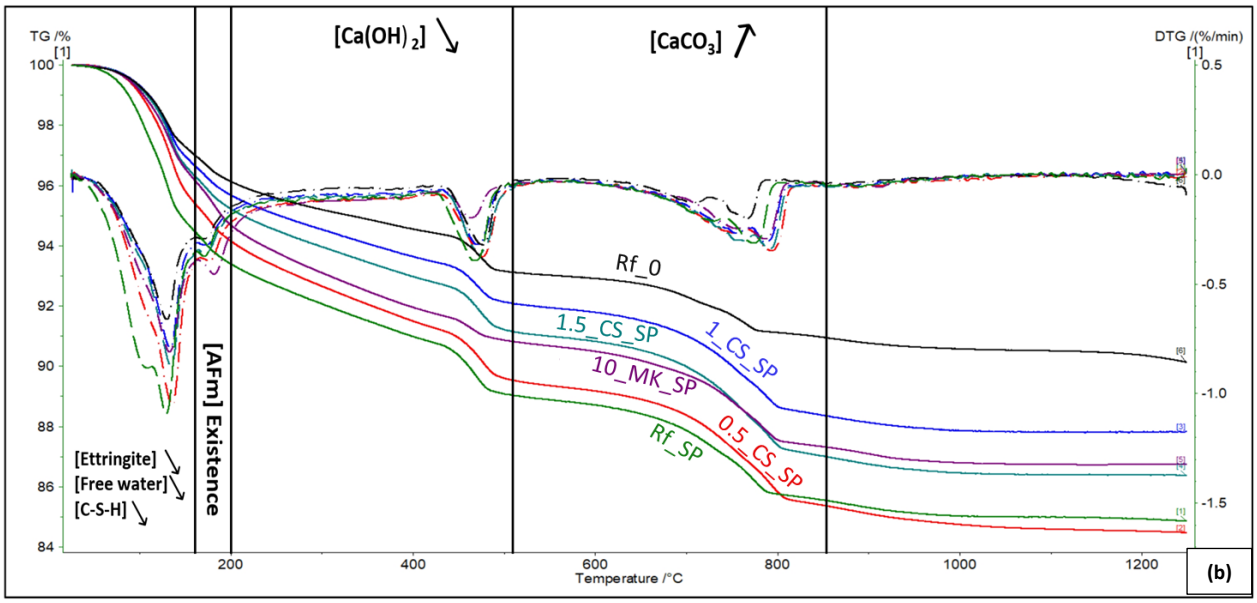

Fig. 7. TGA of mixes (a) without SP and (b) with SP

Table 7. Mass variation of Ettringite, Free water, C-S-H and $Ca(OH)_2$ at 28 day, obtained by TGA test.

Nomination	Mass variation of Ettringite, Free water and C-S-H (%)	Mass variation Portlandite $Ca(OH)_2$ (%)
Rf_0	-3.87	-1.32
Rf	-9.02	-1.75
0.5_CS	-5.17	-1.49
1_CS	-4.95	-1.69
1.5_CS	-4.85	-1.62
Rf_SP	-6.60	-1.77
0.5_CS_SP	-5.85	-1.77
1_CS_SP	-4.32	-1.40
1.5_CS_SP	-4.78	-1.66
10_MK_SP	-5.31	-0.96

3.1.2 Mercury Intrusion Porosimeter analyses (MIP)

MIP tests were performed on ten mortar samples, with and without the addition of SP. This analysis aimed to determine their porous characteristics, including distribution, size, volume and changes in total porosity inducted by the incorporation of CA fibers, CS and MK. These results were then compared to those of the reference mortars. In previous research by the authors, it was observed that incorporating CA into the cementitious matrix resulted in similar microstructural properties for the surface, core and intermediate parts of the mortar. Therefore, the microstructure analysis was focused on the core section of the mortar.

In **Fig. 8**, the pore volume is plotted against the pore size diameter for mixes without SP (**Fig. 8a**), and with SP (**Fig. 8b**). The pore sizes range from 3.6 nm to 430 µm and are classified into three

categories: i) gel pores (3.6 nm and 10 nm), ii) capillary pores (10 nm and 1 µm) and iii) macropores (1 µm and 430 µm). In the case of the reference mortar Rf_0, two major peaks are observed, and the pore size distribution tends toward a bimodal distribution centred between 35 – 175 nm. However, for Rf and Rf_SP, after the addition of CA, pore diameters become more dispersed and heterogeneous, leading to a plurimodal pore size distribution.

A decrease in capillary pore volume (with a peak between 30 and 300 nm) is observed, decreasing from 0.1 mL/g for Rf_0 to values below 0.04 mL/g for all other mixes. This finding shows a decline in the number of connected pores within the capillary pore size range. The authors in [65] attribute this reduction to the addition of CS. In the authors' earlier findings, it was observed that an increase in sand replacement by CA in mortars led to a gradual decrease in pore volume within the 30 to 300 nm range. Thus, in this study, the reduction in connected pores is also associated with the addition of CA fibers.

Fig. 9 illustrates the variation in porosity volume in three different pore size ranges [66]: gel pores (1 nm – 10 nm), capillary pores (10 nm – 1 µm), and macropores (>1 µm). The quantity of pores with a diameter greater than 1 µm and less than 10 nm tends to increase (**Fig. 9**). As concluded in [37], this change may be attributed to the creation of a transition zone between CA and cement paste. When comparing the impact of CA and CS, it is evident that CS has a secondary effect on the microstructure. The total porosity of the mortars exhibits a slight variation ranging from 14.5% to 17.4%. This variation can be attributed to the morphology of CA fibres, which can agglomerate within the mixture [37]. Among the mixes without SP (**Fig. 9a**), 1.5_CS exhibits the lowest porosity, equal to 14.5%, closely approaching the Rf value of 14.6%. The total porosity of these mixes progressively decreases as the CS content increases from 0.5 to 1 to 1.5%. When CS is added, the total porosity of the mortars becomes higher than the references without SP which are Rf_0 and Rf, except for 1.5_CS. In the case of mixes with SP, the lowest total porosity is recorded for 1_CS_SP, equal to 14.6%. The total porosity of 0.5_CS_SP and 1.5_CS_SP is higher than the references Rf_0 and Rf_SP. The difference observed in porosity variation when adding CS indicates that CS alters the pores characteristics [61]. When comparing mixes with the same CS rate, the ones with SP (**Fig. 9a**) exhibit slightly greater porosity than those without SP (**Fig. 9b**), except for 1% CS (1_CS_SP). Adding CS in the presence of SP slightly increases the quantity of pores with a diameter less than 1 µm (gel pores + capillary pores), compared to mixes without SP. Additionally, it has been found in [61] that when the CS rate exceeds 1%, pore formation is promoted. Therefore, it can be concluded that in the presence of SP, CS has the potential to impact the microstructure by slightly increasing the total porosity.

When comparing the pore volume within each pore category in **Fig. 9(a-b)**, it can be deduced that the addition of CA alone leads to a decrease in the number of capillary pores (with a diameter ranging from 10 nm to 1 µm) compared to the reference Rf_0. The addition of CA results in the transformation of some capillary pores into smaller pores: micropores (with a diameter less than 10 nm) and larger pores: macropores (with a diameter exceeding 1 µm). In [37], the presence of a transition interfacial zone around the fibres in the cement matrix may explain the variation in pore categories. Furthermore, the addition of CS in the presence of CA tends to reduce capillary pore values when compared to Rf_0. Similar findings were reported when CS was added to concrete mixes in [59] and [67]. This reduction is attributed to the formation of a wax-like

compound resulting from the reaction between CS and portlandite, which persists within the capillary pores in the form of a hydrophobic layer on the pore walls during the hydration process [68]. Therefore, the diameter of capillary pores decreases with the addition of CS.

In reference to the metakaolin mix, **Fig. 9b** illustrates that 10_MK_SP exhibits the lowest quantity of capillary pores (44.1%) and the highest proportions of gel pores and macropores, respectively 28.9% and 27%, compared to the other mixes. The addition of metakaolin in 10_MK_SP refines its pore microstructure compared with the other mixes [69], [70], [71].
In [72], it was shown that pore size significantly influences mortars mechanical strength . A direct correlation between pore size and mechanical strength was obtained. Additionally, findings in [61] reveal that larger pores have a more harmful effect on mechanical strength, as they tend to promote crack formation. Section 3.2 will address the impact of CA and CS on mortars at the macroscopic scale.

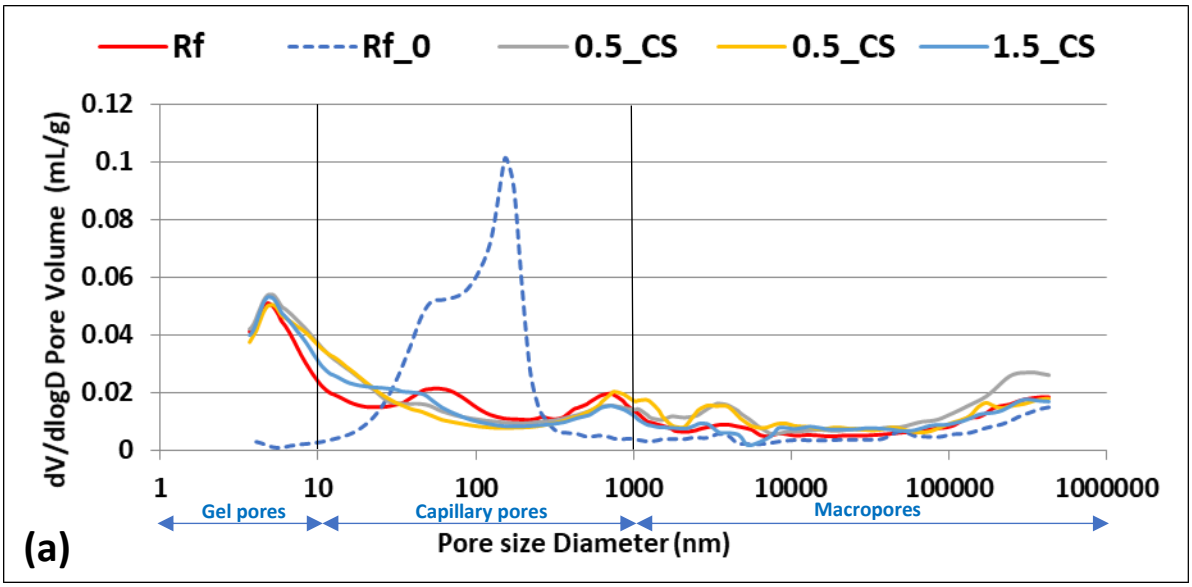

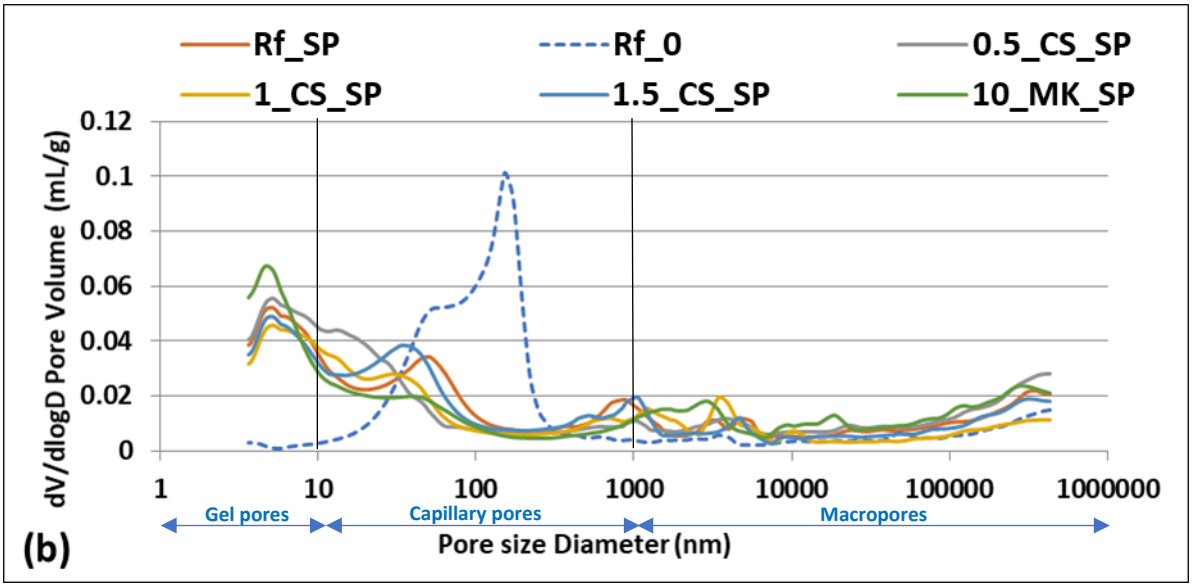

Fig. 8. Pore size distribution of mixes (a) without SP, (b) with SP.

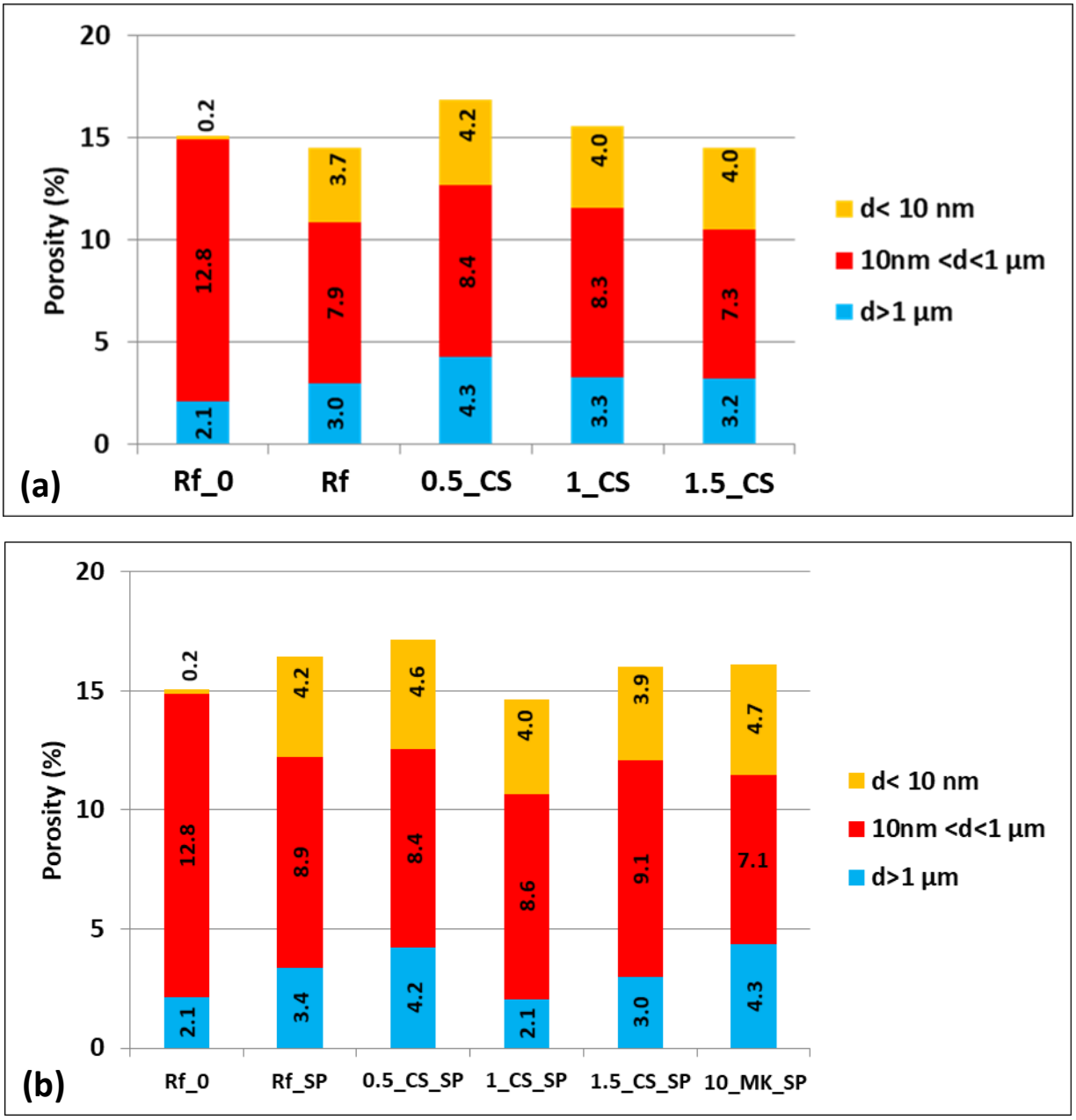

Fig. 9. Variation of the pores volume of mortars in different pore range for mixes (a) without SP and (b) with SP in terms of porosity.

3.1.3 Scanning electron microscope (SEM)

Microstructural analyses were conducted on mortars containing SP. The images in **Fig. 10** represent microscopic observations of the following samples: (a) Rf_SP, (b) 10_MK_SP, (c, d) 0.5_CS_SP, (e, f) 1_CS_SP and (g, h) 1.5_CS_SP.

In **Fig. 10b,** metakaolin plays a key role in pore filling, leading to the development of a finer microstructure compared to Rf_SP (**Fig. 10a**). When comparing the microstructure of the CS-mixes to that of Rf_SP (**Fig. 10 a**), CS agglomerates are detected (**Fig. 10e**). These CS agglomerates contribute to a tendency of reducing some capillary pores (**Fig. 10c**), as previously observed in MIP tests. Due to its fibrous and fluffy texture, resembling cotton fibers, CA displays a cottony appearance, leading to the incomplete coverage of CA fibers by CS (**Fig. 10d**). Furthermore, as the quantity of CS increases, the presence of agglomerates formed by CA and CS becomes apparent, as observed in **Fig. 10h** when compared to 0.5_CS_SP illustrated in **Fig. 10c**. In **Fig. 10g,** there is a notable rise in the quantity of free CS particles, those not adhering to CA fibres, corresponding to the increased CS content compared to **Fig. 10(c-e)**, contributing to the increase in small pores. This observation indicates that free CS particles will create more small pores, that tend to merge, and create larger voids making the mix less compact. It is pertinent to note that a similar finding was reported in [61].

It can be seen that CS weakens the bond between the cement paste components, resulting in the formation of a transition zone between CA fibers and the cement paste, as illustrated in **Fig. 10f**. This leads to an increase in the number of voids and pores, which support the findings from previous MIP results on mortars with SP. In the literature, it has been observed that the addition of CS in mixes leads to the development of an interfacial transition zone (ITZ) [65]. As previously mentioned in [67], [73], the obtained results indicate that CS negatively impacts the microstructure in the presence of SP. In the mixes containing CS (**Fig. 10c-h**), the transition zone between CA fibers and the cementitious matrix appears larger than the transition zone between CA fibers and the cementitious matrix in the reference mix, Rf_SP (**Fig. 10a**). When CS is added, the bond between sand aggregates and the cement paste appears weakened.

Furthermore, CS incorporation results in cracks formation in both the cement paste and the ITZ (**Fig. 10f**), as observed in [73].

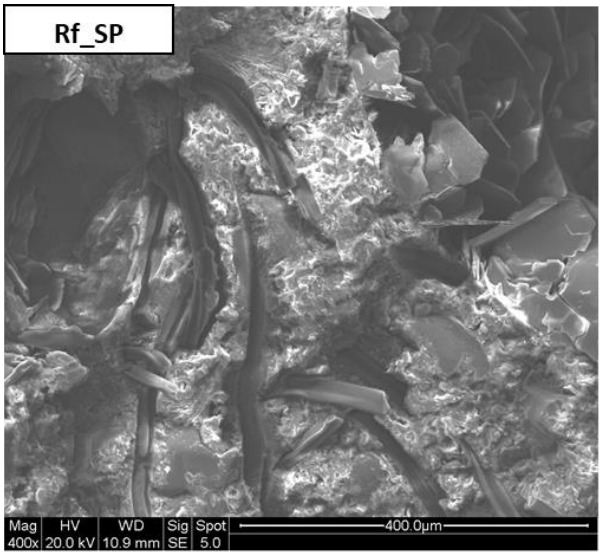
Rf_SP
Mag HV WD Sig Spot
400x 20.0 kV 10.9 mm SE 5.0
400.0µm

(a)

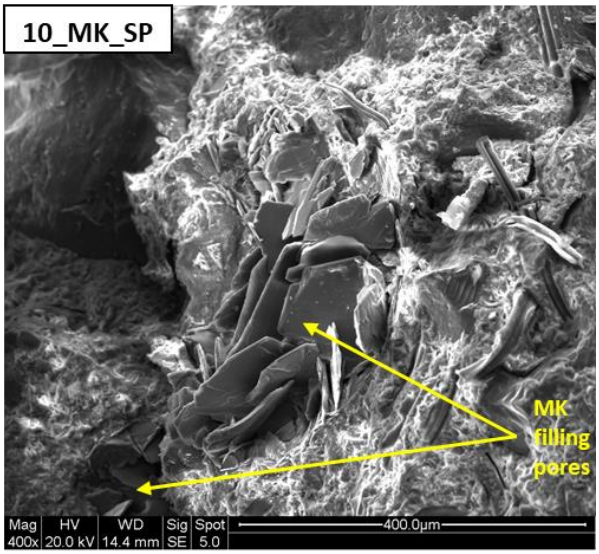
10_MK_SP
MK filling pores
Mag HV WD Sig Spot
400x 20.0 kV 14.4 mm SE 5.0
400.0µm

(b)

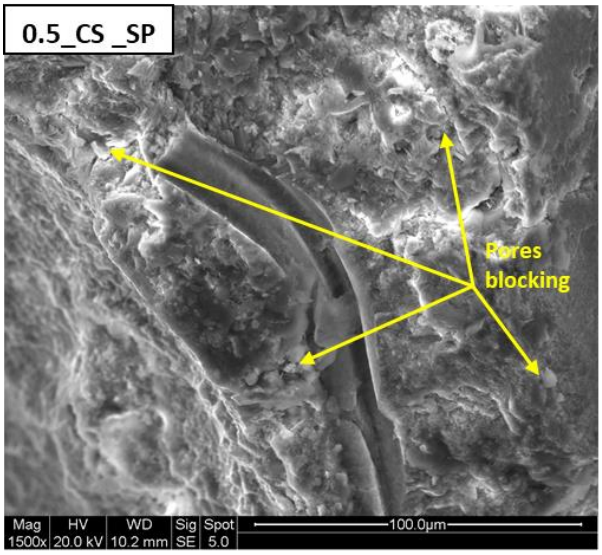
0.5_CS _SP
Pores blocking
Mag HV WD Sig Spot
1500x 20.0 kV 10.2 mm SE 5.0
100.0µm

(c)

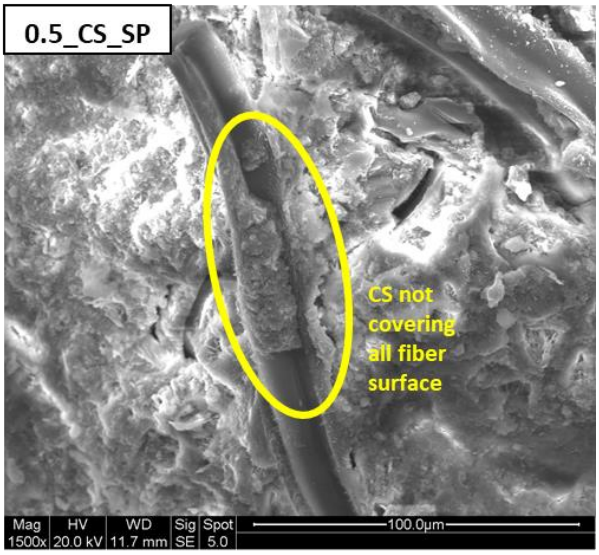
0.5_CS_SP
CS not covering all fiber surface
Mag HV WD Sig Spot
1500x 20.0 kV 11.7 mm SE 5.0
100.0µm

(d)

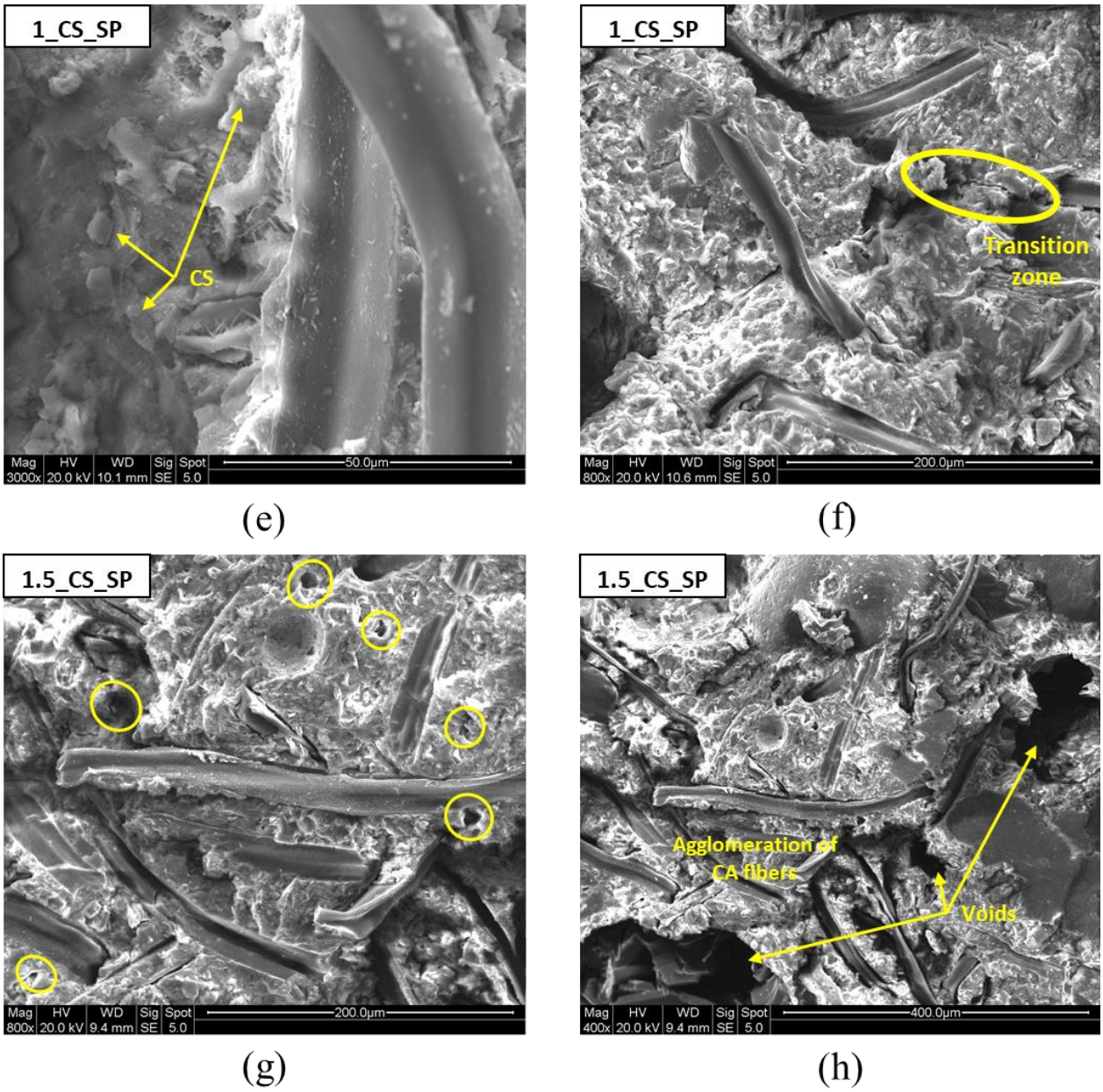

Fig. 10. SEM micrographs of mortars with SP.

3.2. Macrostructural properties

3.2.1 Workability

Fig. 11a & **Fig. 11b** illustrate the workability of the mixes. The reference mix, Rf_0, demonstrated a slump of 11.1 mm, as expected for a standard mortar. In the mixes produced without SP (**Fig. 11a**), the workability dropped by 91% upon the addition of CA fibers. As confirmed in authors' previous study, when fibers are incorporated at a rate exceeding 0.2 wt%, it results in dry mixes due to the absorption of water by CA. With the introduction of CS, the workability of the mixes dropped to zero. According to [42] regarding concrete fresh properties, CS incorporation

increases the air content, leading to a decrease in workability. This is attributed to the formation of a hydrophobic layer. The addition of SP (**Fig. 11b**) was therefore essential to enhance the mixes workability . The highest workability was achieved in the reference mix Rf_0_SP, where the SP increased workability to 143.5 mm. SP generates a repulsive force between particles that prevents agglomeration [74].

Workability gradually decreases with increasing CS content. As CS content increases from 0.5 wt% to 1.5 wt% of cement, the workability of the mixes decreases from 23 mm to 5 mm. In [67], the authors observed a direct correlation between the workability reduction and the incorporation of CS at certain w/c ratios. Their findings indicate that CS influences air content more significantly at w/c ratios 0.35 and 0.45.

When manually mixing 0.5 CS wt% along with CA fibers, it became apparent through microscopic observations in **Fig. 5 & Fig. 10b**, that this amount of CS is insufficient to adequately cover the entire surface of the CA fibers, thereby failing to completely reduce their water absorption. Consequently, when increasing CS content from 0.5 to 1%, workability decreased. This increase in CS coverage resulted in a reduced water absorption by the fibers, leading to a decrease in workability, approaching it to the reference Rf_0. The decrease in slump associated with the addition of CS can also be attributed to the irregular shape of CS particles [73]. This irregularity of CS particles is demonstrated in **Fig. 3b**. As a result, increasing the CS content reduce workability. Additionally, CA fibers have a cotton-like appearance due to agglomerations, preventing CS high dispersion. This emphasizes the challenge of ensuring that all fibers are adequately coated, as demonstrated in the SEM observation in **Fig. 5**.

In the case of the 10_MK_SP mix, a slump of 19 mm is obtained, which is a higher value than that of the reference Rf_0. As mentioned in [63], MK is known for its ability to enhance concrete workability through a chemical reaction with cement hydrates, resulting in an improved microstructure. In **Fig. 9b,** it can be observed a modified microstructure in the 10_MK_SP mix. This mortar has the highest content of pore gels and macropores, while having the lowest capillary pores content.

It was assumed that the optimal formulation is the one that yield workability results similar to Rf_0. For the mixes without SP, an optimal formulation cannot be found because all the obtained mixes were dry, lacked cohesion, and had zero slump. However, for the mixes with SP, optimal results were achieved for 1_CS_SP and for the mix containing metakaolin 10_MK_SP.

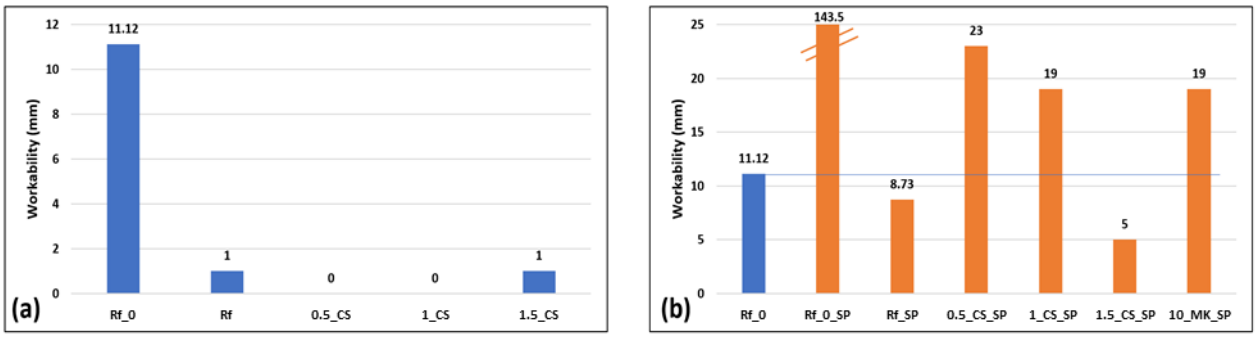

Fig. 11. Workability of mortars without SP (blue), with SP (orange).

3.2.2 Total shrinkage

Three samples were manufactured for each mix to measure the average total shrinkage and its standard deviation. As demonstrated in the previous work by the authors, CA fibers are highly absorbent, leading to variations in the total shrinkage of mortars. CS is added to reduce CA water absorption, as found in TGA results (**Fig. 7b)**. **Fig. 12a** & **Fig. 12b** illustrate two steps: i) a first step marked by significant shrinkage variation, indicating water evaporation and the cement hydration process, and ii) a second step with a gradual increase in shrinkage but with smaller slopes. The observed shrinkage can result from both chemical shrinkage during the advanced stage of hydration and drying shrinkage due to gradual water loss over time. However, this drying shrinkage occurs at a slower rate than during the initial drying period caused by the presence of less free-water [75], [76]. According to [75], the water absorbed by cellulose fibers continues to evaporate even after the initial drying period, mainly due to the progressive release of water from both the internal pores and the fiber surface.

In the mixes without SP (**Fig. 12a**), the addition of CA and CS leads to increased shrinkage compared to Rf_0. The total shrinkage varies from -550 to -930 µm/m. When the fibers alone (Rf) were added, shrinkage increased by 47% compared to Rf_0, reaching -831 µm/m. When comparing the mixes containing CA, there was no significant difference observed between Rf and 0.5_CS. 1.5_CS has the highest shrinkage among all mixes without SP, reaching -927 µm/m. The lowest shrinkage value among the mixes with CS is achieved with 1_CS, reaching -677 µm/m. This value represents the optimal result compared to Rf_0. According to [59], it was found that dosages exceeding 1% CS resulted in increased shrinkage. It can be concluded that without SP, a 1% CS decreases CA mortars shrinkage. However, it is imperative to note that the value remains higher than that of the reference mortar without CA, which is Rf_0.

In the case of mixes with SP (**Fig. 12b**), Rf_0_SP has a significant total shrinkage of approximately -1100 µm/m. This can be attributed to the enhanced fluidity of the mix resulting from the high SP dosage. As mentioned in [77], [78], [79], [80], the addition of SP in mortar and concrete mixes is associated with a shrinkage increase. Given that CA fibers absorb an important quantity of water, it can be deduced that the shrinkage of Rf_0_SP is higher than that of Rf_SP[37]. The water content in the mix decreases leading to a reduction in shrinkage. This observation is also noticed in the mass variation of water in TGA tests, as shown in **Fig. 7b**, when comparing Rf_0 and Rf_SP. When CA and CS are introduced, the total shrinkage decreases as follows: Rf_SP, 1.5_CS_SP and 1_CS_SP have nearly identical values ranging from -800 to -850 µm/m. 0.5_CS_SP displays the lowest shrinkage among the mixes with CS, with a 13% reduction compared to Rf_SP. As is well known, CS reacts with cement and water to create a hydrophobic, wax-like compound. As indicated in [59], the reduction in shrinkage comes from the wax-like compound having a more stable volume during cement hydration than C-S-H. 10_MK_SP achieves optimal results with lower shrinkage values. Furthermore, results in [44], reveal that the addition of metakaolin in various proportions does not have a significant impact on total shrinkage.

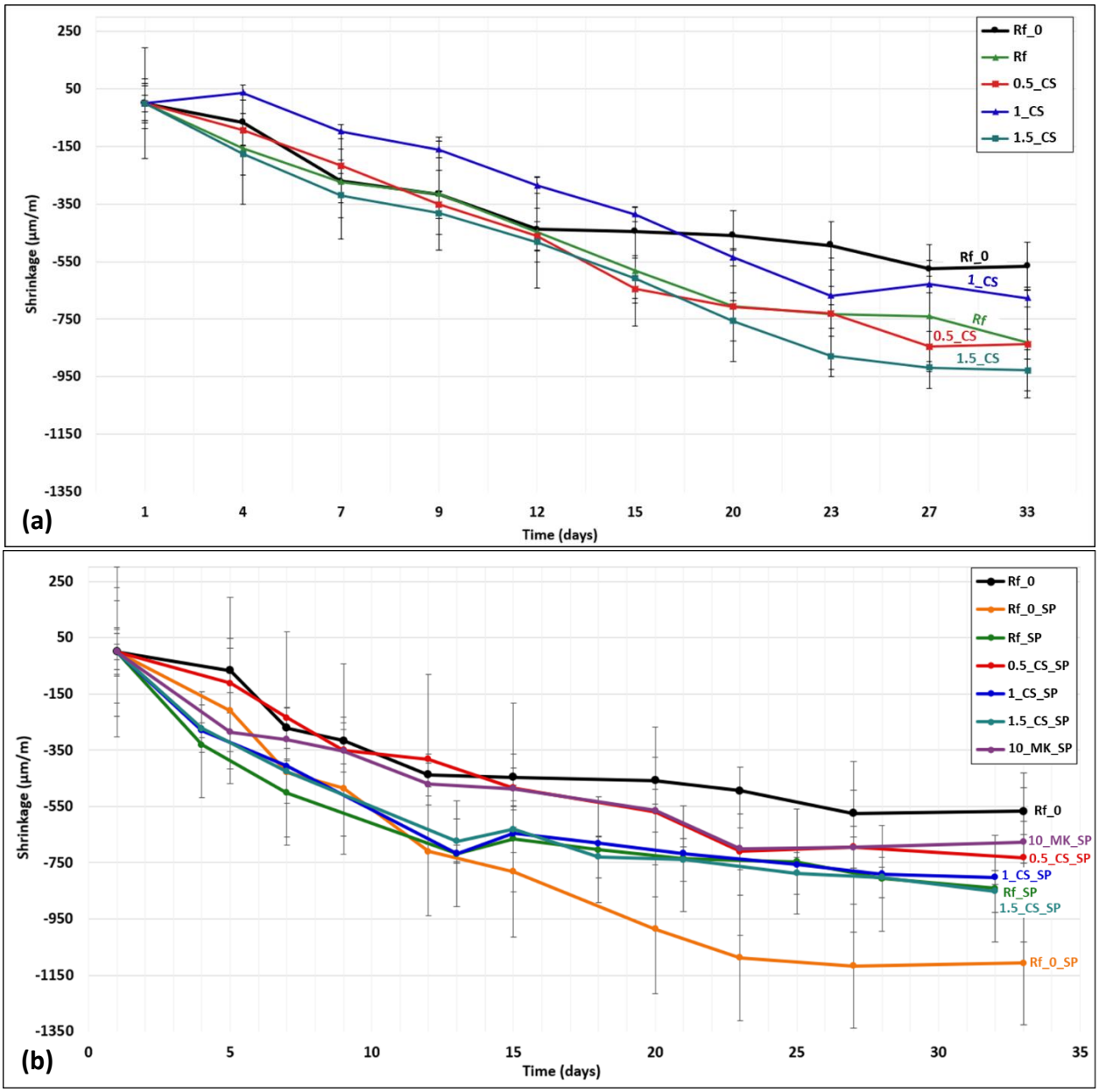

Fig. 12. Total shrinkage of mortars (a) without SP, (b) with SP.

3.2.3 Compression and bending strengths, and water porosity

Fig. 13 presents the compressive and bending strengths and water porosity at 28 days for the manufactured mortars, without SP (**Fig. 13a**) and with SP (**Fig. 13b**), considering different mix designs.

In **Fig. 13a**, despite the very close porosities of Rf_0 and Rf, which are 19.31 ± 0.11% and 19.18 ± 1.09%, respectively, Rf_0 has the highest compressive strength of 44.03 ± 0.91 MPa. However, upon adding CA fibers, the compressive strength decreases by 39.5%, reaching 26.64 ± 1.37 MPa for Rf. After the addition of CS in the mixes, both 0.5_CS and 1.5_CS have nearly the same compressive strengths, around 25 MPa. In contrast, 1_CS has the highest compressive strength among the CS-based mixes, reaching 27.36 ± 1.45 MPa. Mechanical strength decrease is

attributed to dry mixes and lack of cohesion. CA absorbs a portion of cement paste setting water. Meanwhile, the porosity of mixes with CS gradually decreases as CS content increases. These results align with the previous results from TGA tests: among the CS-containing mixes, 1_CS is identified as the optimal value in terms of mass variation of portlandite (**Fig. 7**). Similarly, the optimal shrinkage result is achieved with 1_CS (**Fig. 12**). The bending strength across all the mixes shows a minor variation, ranging from 4 to 5 MPa, except for the reference mortar, which has a bending strength of 7.45 ± 0.2 MPa.

The results of the mechanical properties of the mixes with SP are presented in **Fig. 13b**. Among all the mixes (except the reference Rf_0), 10_MK_SP has the highest compressive strength. It is worth noting that metakaolin not only increases the binder quantity due to its addition to the mix, but also plays a key role in refining the microstructure, as demonstrated in the MIP test in **Fig. 13b**. When comparing mixes with SP (**Fig. 13a**), to those without SP (**Fig. 13b**), It is observed that the addition of SP leads to an increase in compressive strength and a decrease in porosity. For example, 0.5_CS and 1_CS show respective compressive strengths and porosities of 24.5 MPa, 19.35% and 27.36 MPa, 18.47%. After the addition of SP, 0.5_CS_SP and 1_CS_SP, have respectively compressive strengths and porosities of 31.03 MPa, 17.26% and 31.2 MPa, 15.66%. The improvement of workability in the mixes due to SP is consistent with improved mechanical strength and reduced porosity.

The compressive strength of the mixes containing CS (0.5_CS_SP, 1_CS_SP and 1.5_CS_SP) is lower than that of Rf_0 but higher than Rf and Rf_SP. In CS-mixes, CS coats the fibers, reducing water absorption. This results in more water available for cement hydration and, consequently, better compressive strength. Among the CS containing mixes, 1_CS_SP demonstrated the highest mechanical strength and the lowest porosity. As observed in SEM images (**Fig. 10c**), CS agglomerates can reduce certain pores. Excessive use of CS will reduce the Rc. In [65], the decrease in Rc was attributed to possible agglomeration of CS, which negatively affected the mix cohesion.

In the case of mixes with SP (**Fig. 13b**), bending strength decreases with the addition of CA and CS when compared to Rf_0, which has a bending strength of 7.45 MPa. It remains at approximately 5 - 6 MPa for CS mixes. Metakaolin mix provides a slightly higher bending strength of 6.49 MPa compared to the other mixes. This is because metakaolin serves as a filler, allowing it to fill the pores, as demonstrated in MIP results (**Fig. 8b**).

Conflicting results regarding CS impact on mechanical performance can be found in the literature [67]. A number of articles have shown that the use of CS reduced Rc [59], [61], [65], [73]. A relation exists between the reduction in Rc and the incorporation of CS. The decline in mechanical strength is associated with an increase in air content in the fresh state. This effect is attributed to the hydrophobic change, which in turn affects porosity by increasing it and changing the pore size distribution [65], [67]. These modifications were observed in the microstructure experiments. The pore size distribution changed in CS mortars in MIP tests. Higher porosity was observed in the transition zone between fibers – CS – cement paste (**Fig. 10f**). While in [59], the authors established a link between the creation of a hydrophobic layer covering the capillary pores and the reduction in Rc.

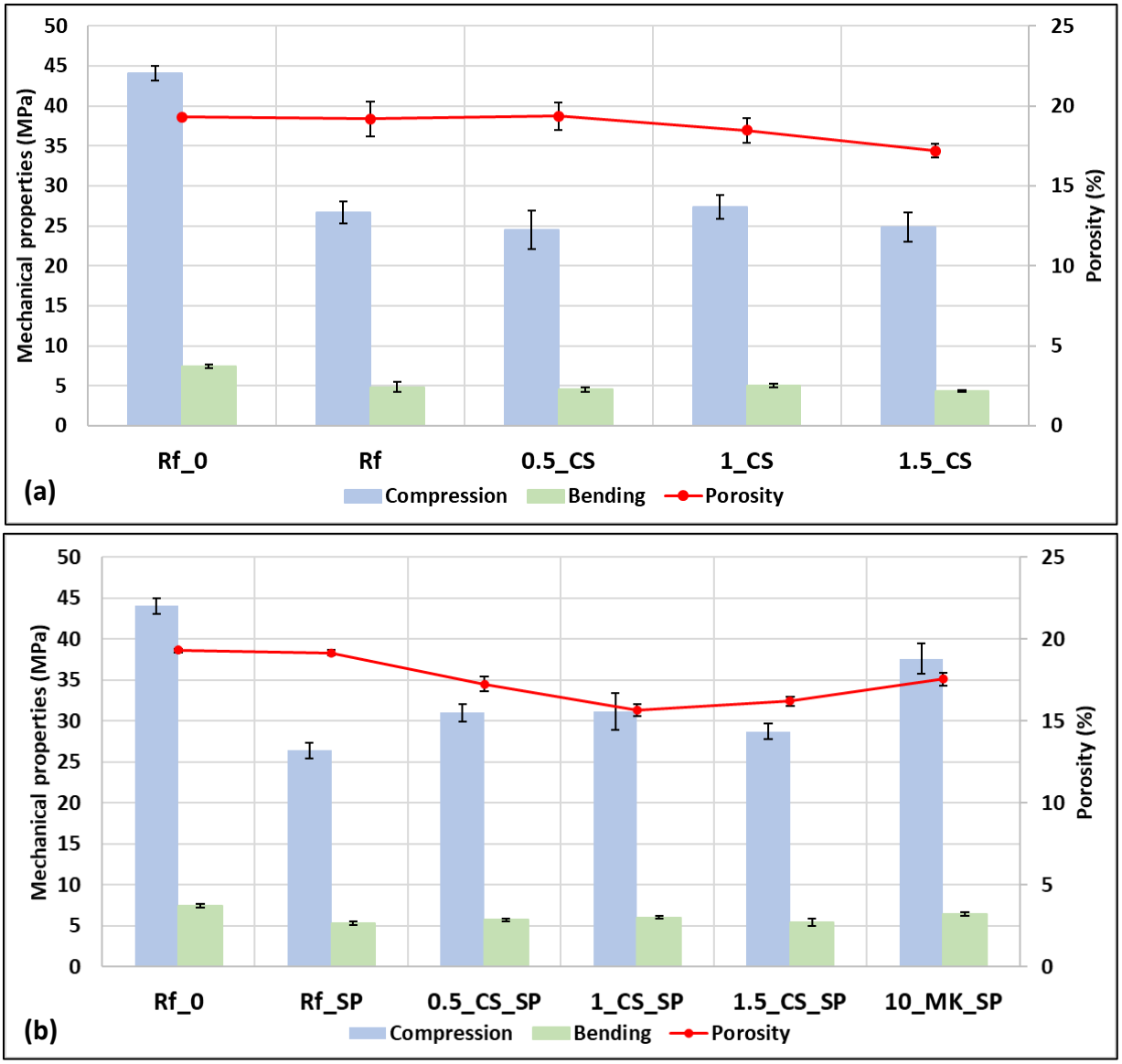

Fig. 13. Compressive strength (in blue), bending strength (in green) and porosity (in red) vs CA based mortars at 28 days for the mixes (a) without SP (b) with SP.

3.2.4 Density

Rf_0 has the highest bulk density of 2135.6 ± 0.01 kg/m^3. CA-based mortars have a porous cementitious matrix, resulting from the high porosity created by the incorporation of CA in the mixes. This contributes to a decrease in density. For instance, the densities of both Rf and Rf_SP (incorporating CA fibers) decreased by 7% compared to Rf_0.

As demonstrated before in SEM observations, CS has the ability to fill some small pores and form agglomerates, leading to a slight increase in density. According to the literature, when CS was added at low dosages (1 kg/m^3 of concrete [67] for example), the density remained nearly constant, with only a slight decrease as the CS amount increased, as noted in [43], [67], [73]. In [59], the decrease in density was attributed to the stearate group's reaction with C–S–H, resulting

in a wax-like compound assumed to be lighter than C–S–H. Moreover, this decrease in sample density was insignificant.

Among CA-based mixes without SP (**Fig. 14a**), the highest bulk density is recorded for 1.5_CS, with a value of 2010.9 ± 0.02 kg/m^3, while the lowest bulk density is observed for 1_CS, measuring 1978 ± 0.01 kg/m^3. The density has slightly increased compared to Rf (**Fig. 14a**), except for 1_CS with a slight decrease.

Among CA-based mixes with SP (**Fig. 14b**), the highest bulk density is observed for 1_CS_SP, with a value of 2019.2 ± 0.02 kg/m^3, while the lowest bulk density is recorded for 10_MK_SP, with a value of 1972.5 ± 0.05 kg/m^3.

A correlation can be established between the bulk density of mixes with SP (**Fig. 14b**), porosity and MIP results. For instance, as the CS rate increased from 0.5 wt% to 1 wt% of cement, the density also increased, leading to a reduction in mortar porosity. In contrast, when 1.5 wt% of CS was added, the density decreased while the porosity increased. The density slightly surpasses that of Rf_SP after the addition of CS.

However, the application of CS coating to CA fibers hasn't significantly impacted the density. The addition of both CA fibers and CS reduces the density, caused by CA addition.

A correlation can be established between TGA results and bulk density. In [67], the authors observed that an increased concentration of $Ca(OH)_2$ leads to lower densities in mortars containing CS. As represented in **Fig. 14b**, Rf_SP and 0.5_CS_SP have identical densities of 1986 kg/m^3, along with matching mass changes for $Ca(OH)_2$ equal to 1.77%.Furthermore, 1.5_CS_SP demonstrates a higher density compared to 0.5_CS_SP (2005 ± 0.01 kg/m^3), with a mass change of approximately 1.66%. 1_CS_SP has the highest density among the CS containing mixes of 2019.2 ± 0.02 kg/m^3, while having the lowest $Ca(OH)_2$ mass loss among these mixes, equal to 1.4%. Lower densities result from an increase in $Ca(OH)_2$ content because it weakens the bonding between aggregates and the paste [67].

The density results of the mixes with SP (**Fig. 14b**) are consistent with the previous porosity and mechanical strength results. For example, 1_CS_SP has the highest bulk density: 2019.2 ± 0.02 kg/m^3, the lowest porosity: 15.66% and the greatest compressive strength: 31.2 ± 2.23 MPa. However, it should be noted that bulk density is not the only factor influencing mechanical strength [67].

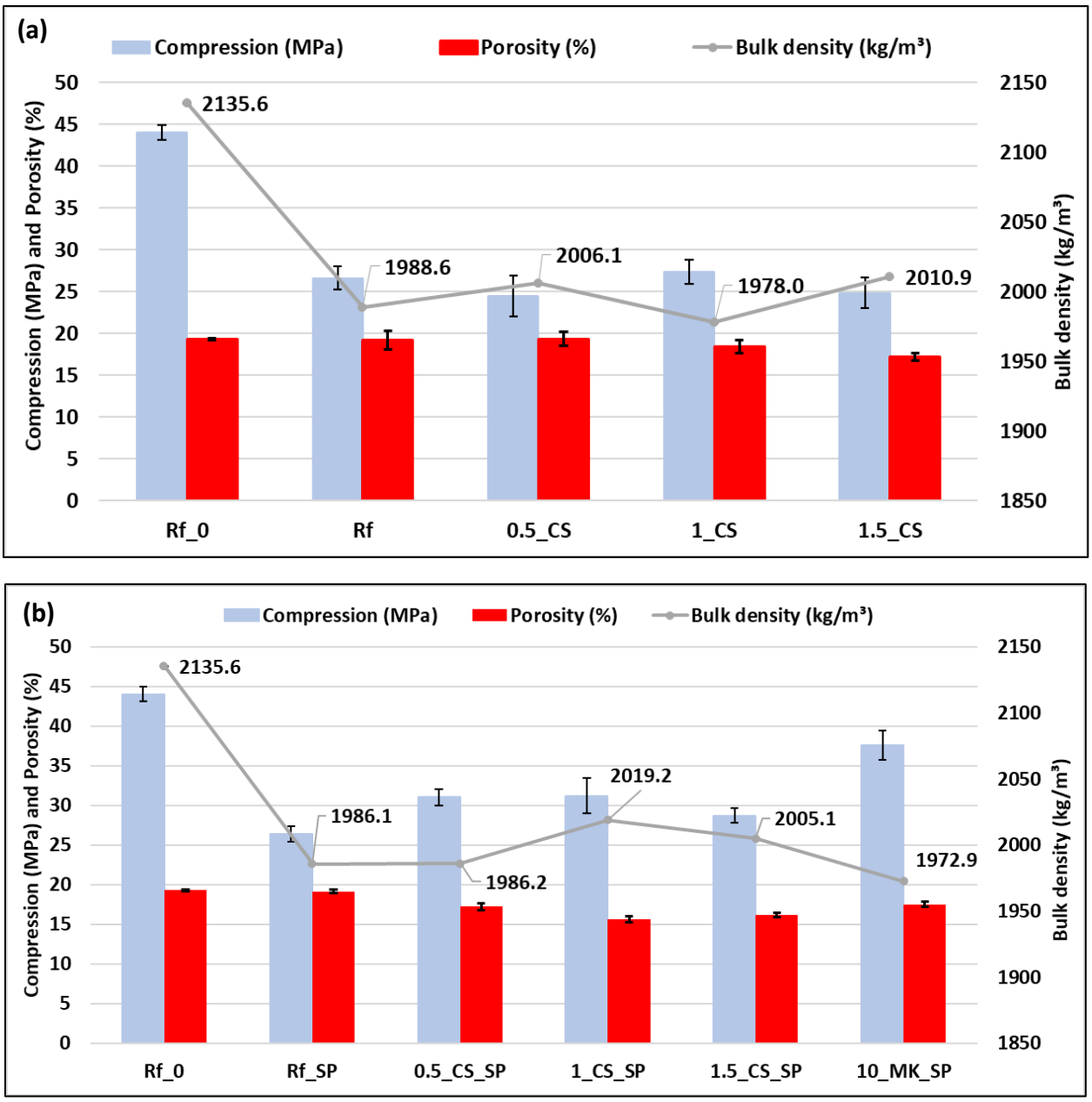

Fig. 14. Bulk density (in grey), Compression (in blue) and porosity (in red) of mortars (a) without SP and (b) with SP as function of the replacement rate.

3.3 Discussion

Table 8 summarizes the bulk density, mechanical properties, shrinkage and porosity (WAPT, MIP) for the studied CA-based mortars.

It can be seen that 10_MK_SP has better mechanical properties than other CA-based mixes with the highest compressive and bending strengths of 37.61 ± 1.87 MPa and 6.49 ± 0.21 MPa, respectively. Additionally, it demonstrates the lowest shrinkage of 677 ± 75 µm/m. Metakaolin has been observed to refine the microstructure, leading to improved mechanical strengths.

When comparing the shrinkage of the mixes to that of the reference Rf_0, it appears that the addition of both CA and CS increases shrinkage. Furthermore, among CA mortars, it was observed that the addition of less than 1% CS resulted in better shrinkage outcomes. This result can be attributed to CS particles coating CA fibers, thereby reducing their water absorption.
The reduction in mechanical strength is attributed not only to CA addition but also to the incorporation of CS. All mixes containing CS (at rates of 0.5%, 1% and 1.5 % rates) have lower compressive strength and bending strength compared to Rf_0. This decrease is associated to the creation of a hydrophobic layer that coats the fibers. Additionally, this layer leads to the formation of CS agglomerates, as observed in SEM images. It tends to increase the air content in the fresh state. The hydrophobic layer changes the pore distribution and the total porosity. SEM findings indicate that 1_CS_SP has the highest compressive strength and the lowest porosity, as CS can block smaller pores. Furthermore, 1_CS_SP has the highest bulk density, 2019.2 ± 0.02 kg/m³, resulting in better mechanical performance.

The mixes with SP have higher compressive and bending strengths and lower porosity compared to the mixes without SP. The use of SP results in improved workability and mechanical strength, along with reduced porosity. Mortar density increases when the CS rate is raised from 0.5% to 1%. This rise can be attributed to the increased CS content from 0.5 to 1 wt%, resulting in decreased porosity.

Table 8. Mortar properties for the mixes without/with SP.

Formulations	Bulk Density (kg/m³)	Compressive strength (MPa)	Bending strength (MPa)	Total Shrinkage (µm/m)	Porosity from WAPT (%)	Porosity from MIP (%)
Rf_0	2135.6 ± 0.01	44.03 ± 0.91	7.45 ± 0.2	566 ± 84	19.31 ± 0.11	15.02
Rf	1988.6 ± 0.02	26.64 ± 1.37	4.85 ± 0.63	831 ± 193	19.18 ± 1.09	14.52
0.5_CS	2006.1 ± 0.01	24.5 ± 2.42	4.54 ± 0.25	837± 52	19.35 ± 0.43	16.87
1_CS	1978 ± 0.01	27.36 ± 1.45	5.08 ± 0.23	677 ± 30	18.47 ± 0.77	15.59
1.5_CS	2010.9 ± 0.02	24.86 ± 1.83	4.38 ± 0.10	927 ± 71	17.19 ± 0.42	14.49
Rf_0_SP	-	-	-	1106 ± 219	-	-
Rf_SP	1986.1 ± 0.02	26.42 ± 0.98	5.35 ± 0.21	842 ± 190	19.17 ± 0.19	16.43
0.5_CS_SP	1986.2 ± 0.01	31.03 ± 1.06	5.74 ± 0.14	731 ± 299	17.26 ± 0.76	17.15
1_CS_SP	2019.2 ± 0.02	31.2 ± 2.23	6.04 ± 0.16	802 ± 24	15.66 ± 0.35	14.63
1.5_CS_SP	2005.1 ± 0.01	28.74 ± 0.94	5.41 ± 0.42	852 ± 74	16.21 ± 1.21	16.02

10_MK_SP	1972.9 ± 0.05	37.61 ± 1.87	6.49 ± 0.21	677 ± 75	17.55 ± 0.37	17.38

To investigate the relationships between the properties of CA-based mortars and the different rates of additives (SP, MK and CS), a correlation analysis (Table 9) was conducted using the XLSTAT software integrated within Excel. The Pearson correlation coefficient was calculated for all variables, ranging from -1 to 1. A coefficient of 1 indicates a perfect positive linear relationship, -1 indicates a perfect negative linear relationship, and 0 indicates no linear relationship. From Table 9, it can be observed that:

- The addition of MK, improves the mechanical properties and the microstructure (MIP results) of CA-based mortars manufactured with SP, confirming the initial observations and highlighting the effect of these additives (MK and SP) on the mortar's microstructure and performance.
- CS has a positive impact on the mortars' total shrinkage.
- Despite the addition of CS, MK and SP, no significant differences were noticed for the bulk density.

Table 9. Pearson correlation analysis between the different variables.

	Bulk Density	Compression	Bending	Total Shrinkage	WAPT	MIP
SP	-0.34	0.13	0.31	0.06	-0.59	0.48
MK	-0.27	0.42	0.36	-0.31	-0.10	0.49
CS	-0.14	-0.43	-0.43	0.48	-0.68	-0.30

Accordingly, the studied mortars could be used for various applications, such as cement mortars and bricks in masonry structures. In accordance with NF DTU 26.1 [81], the French standard that defines the requirements for designing and constructing masonry structures with cement-based mortars, the following conditions must be met: i) the compressive strength should exceed 12.5 MPa at 28 days ii) The bending strength must be greater than 0.4 MPa at 28 days, iii) the maximum allowable shrinkage is approximately 0.8 mm/m and iv) the porosity must be maintained at a value lower than or equal to 30%.

Furthermore, according to NF EN 772-1+A1 [82], bricks must have a minimum compressive strength of at least 7.5 MPa. According to NF EN 772-13[83], brick porosity should not exceed 23%. Lastly, NF EN 771-1+A1 [84] sets the maximum allowable linear shrinkage for facing bricks at around 0.6%. It is worth noting that all the studied formulations meet these specified criteria.

Finally, from an environmental perspective, the utilization of cellulose acetate fibers in the construction sector has the potential to reduce the impact on global warming by decreasing the carbon footprint of mortars. A study conducted in [85] focused on CO_2 emissions in mortar production using CA fibers derived from cigarette filters. The researchers observed a significant decrease in environmental impact. For instance, by increasing the CA rate to 1.5 wt%, CO_2-eq emissions decreased by 38.27 CO_2-kg/1000 m^3 compared to the reference mortar.

4. Conclusion

Earlier findings by the authors [37] demonstrated that incorporating cellulose acetate fibers (CA) into standard mortar at a rate of 1.3% by weight of sand increases porosity and shrinkage while decreasing the mechanical strength of the mortar. This effect is attributed to the high water absorption by CA. Therefore, calcium stearate (CS), a damp-proofing admixture, is used to coat the CA fibers. CS powder is mixed with CA fibers before mixing them with cement, water, sand, and a superplasticiser at 3wt% of cement, if workability improvement is needed for some mixes. Then, the macroscopic and microscopic properties of the resulting cementitious mortar mixes are investigated.
Additionally, to enhance mechanical performance, the impact of adding 10 wt% metakaolin by weight of cement is examined.

The following results were obtained:

- TGA analysis demonstrates that the addition of CS reduces the water absorption of CA fibers, with an optimal addition of 1 wt% CS by weight of cement.
- CA and CS additions leads to :
  1- Shift the pore size distribution to plurimodal.
  2- A tendency toward reducing the amount of connected pores when compared to the CA reference mortar with SP (Rf_SP).
  3- Generate more pores in the cementitious matrix.
  4- The formation of agglomerations of these two elements.
- CS does not adhere properly to CA fibers leading to the development of small pores and a weak bond between cement paste particles.
- CS addition reduces the presence of interconnected capillary pores within the pore size range of 10 nm and 1 µm.
- 1 wt% of CS is considered optimal for reducing mortars total shrinkage in both cases, with and without superplasticizer. The incorporation of 10 wt% metakaolin (MK) results in the closest shrinkage value to that of the reference mortar (Rf_0).
- Despite a decrease of the mechanical strength of mortars with admixtures compared to the reference; the optimal mechanical results (for mixes manufactured with CS) are obtained with 1 wt% of CS with and without SP (1_CS, 1_CS_SP). 10_MK_SP achieves the best results with a 15% decrease.
- Coating CA fibers with CS does not significantly impact the mortar dry density.

The results obtained in this study reveal an innovative development in the construction industry, particularly in masonry structures and brick production. Notably, the produced product not only meets the allowable values for the precited applications but also showcases a remarkable opportunity to address environmental concerns by incorporating CA from cigarette butt waste. Looking to the future, further experimental campaigns are essential to develop the use of CA in construction, such as:

- Examining air-based curing method in parallel with water-curing method for CA-based mortars to better align with real-world applications;
- Evaluating CA-based mortars hygrothermal properties;
- Ensuring the durability of CA-based mortars;

- Conducting additional tests varying the SP content to achieve a targeted consistency across all mortar mixes.
- Conducting the life cycle analyses to identify the environmental impact of incorporating CA in the construction sector.

Acknowledgments

The authors would like to thank the technical teams of UMR MCD at Université Gustave Eiffel for all their effort and support. The authors would like also to thank the director of MéGO!, Mr Bastien Lucas, for providing the depolluted CA fibers.

References

[1] World Business Council for Sustainable Development, « Removing carbon responsibly: A guide for business on carbon removal adoption ». septembre 2023. [En ligne]. Disponible sur: https://www.wbcsd.org/gdso2

[2] S. Kaza, L. C. Yao, P. Bhada-Tata, et F. Van Woerden, *What a Waste 2.0: A Global Snapshot of Solid Waste Management to 2050*. Washington, DC: World Bank, 2018. doi: 10.1596/978-1-4648-1329-0.

[3] L. Haeusler, J. Talpin, M. Hestin, et C. Mathery, « Déchets chiffres-clés. L'essentiel 2021 », France, 2021.

[4] H. J. Law et D. E. Ross, « International Solid Waste Association's "closing dumpsites" initiative: status of progress », *Waste Manag. Res. J. Int. Solid Wastes Public Clean. Assoc. ISWA*, vol. 37, n° 6, p. 565-568, juin 2019, doi: 10.1177/0734242X19845755.

[5] E. Efficiency, « Building The global exchange for energy efficiency policies, data and analysis », IEA. [En ligne]. Disponible sur: https://www.iea.org/topics/energyefficiency/buildings

[6] M. Saad, « Potentiel des fibres végétales courtes dans l'amélioration du comportement mécanique des mortiers », These de doctorat, Toulouse, INSA, 2022. [En ligne]. Disponible sur: https://www.theses.fr/2022ISAT0013

[7] Ministère de la Transition écologique., « Ministère de la Transition écologique », Construction et performance environnementale du bâtiment. [En ligne]. Disponible sur: https://www.ecologie.gouv.fr/construction-et-performance-environnementale-du-batiment

[8] M. A. Stumpf, F. Flach, J. R. Pires, et M. P. Kulakowski, « Acoustic Absorption of Mortar Composites with Waste Material », *Arch. Acoust.*, vol. 38, n° 3, Art. n° 3, 2013.

[9] A. Kueh, A. Razali, Y. Lee, S. Hamdan, I. Yakub, et N. Suhaili, « Acoustical and mechanical characteristics of mortars with pineapple leaf fiber and silica aerogel infills – Measurement and modeling », *Mater. Today Commun.*, vol. 35, p. 105540, juin 2023, doi: 10.1016/j.mtcomm.2023.105540.

[10] Y. X. Chen, F. Wu, Q. Yu, et H. J. H. Brouwers, « Bio-based ultra-lightweight concrete applying miscanthus fibers: Acoustic absorption and thermal insulation », *Cem. Concr. Compos.*, vol. 114, p. 103829, nov. 2020, doi: 10.1016/j.cemconcomp.2020.103829.

[11] M. Rahim, O. Douzane, A. D. Tran Le, et T. Langlet, « Effect of moisture and temperature on thermal properties of three bio-based materials », *Constr. Build. Mater.*, vol. 111, p. 119-127, mai 2016, doi: 10.1016/j.conbuildmat.2016.02.061.

[12] H. Binici, O. Aksogan, et C. Demirhan, « Mechanical, thermal and acoustical characterizations of an insulation composite made of bio-based materials », *Sustain. Cities Soc.*, vol. 20, p. 17-26, janv. 2016, doi: 10.1016/j.scs.2015.09.004.

[13] P. Zhu *et al.*, « Study of physical properties and microstructure of aerogel-cement mortars for improving the fire safety of high-performance concrete linings in tunnels », *Cem. Concr. Compos.*, vol. 104, p. 103414, nov. 2019, doi: 10.1016/j.cemconcomp.2019.103414.

[14] F. Pittau, F. Krause, G. Lumia, et G. Habert, « Fast-growing bio-based materials as an opportunity for storing carbon in exterior walls », *Build. Environ.*, vol. 129, p. 117-129, févr. 2018, doi: 10.1016/j.buildenv.2017.12.006.

[15] M. Chougan, S. H. Ghaffar, M. J. Al-Kheetan, et M. Gecevicius, « Wheat straw pre-treatments using eco-friendly strategies for enhancing the tensile properties of bio-based polylactic acid composites », *Ind. Crops Prod.*, vol. 155, p. 112836, nov. 2020, doi: 10.1016/j.indcrop.2020.112836.

[16] A. Sellami, D. Bouayad, A. Benazzouk, S. Amziane, et M. Merzoud, « Study of toughness and thermal properties of bio-composite reinforced with diss fibers for use as an insulating material », *Energy Build.*, vol. 276, p. 112527, déc. 2022, doi: 10.1016/j.enbuild.2022.112527.

[17] V. V. Ribeiro *et al.*, « Cigarette butts in two urban areas from Brazil: Links among environmental impacts, demography and market », *Environ. Res.*, vol. 213, p. 113730, oct. 2022, doi: 10.1016/j.envres.2022.113730.

[18] J. Drope et N. W. Schluger, *The tobacco atlas*, Sixth. Atlanta, Georgia 30303 USA: RR Donnelley, 2018.

[19] J. Mackay, M. Eriksen, et O. Shafey, « The Tobacco Atlas, 2nd American Cancer Society », Atlanta,GA, 2006.

[20] A. Rodgman et T. A. Perfetti, *The Chemical Components of Tobacco and Tobacco Smoke*. CRC Press, 2008. doi: 10.1201/9781420078848.

[21] S. Marinello, F. Lolli, R. Gamberini, et B. Rimini, « A second life for cigarette butts? A review of recycling solutions », *J. Hazard. Mater.*, vol. 384, p. 121245, févr. 2020.

[22] M. I. Romero-Gómez, R. V. Silva, M. F. Costa-Pereira, et I. Flores-Colen, « Thermal and mechanical performance of gypsum composites with waste cellulose acetate fibres », *Constr. Build. Mater.*, vol. 356, p. 129308, nov. 2022, doi: 10.1016/j.conbuildmat.2022.129308.

[23] H. Kurmus et A. Mohajerani, « The toxicity and valorization options of cigarette butts », *Waste Manag.*, vol. 104, p. 104-118, mars 2020, doi: 10.1016/j.wasman.2020.01.011.

[24] M. Yousefi, M. Kermani, M. Farzadkia, K. Godini, et J. Torkashvand, « Challenges on the recycling of cigarette butts », *Environ. Sci. Pollut. Res. Int.*, vol. 28, n° 24, p. 30452-30458, juin 2021, doi: 10.1007/s11356-021-14058-3.

[25] H. Kurmus et A. Mohajerani, « A Continuation Study on Recycling Cigarette Butts in Fired Clay Bricks », School of Engineering, RMIT University, 2020.

[26] Official Journal of the European Union, *Directive 2014/40/EU of the European Parliament and of the Council of 3 April 2014 on the approximation of the laws, regulations and administrative provisions of the Member States concerning the manufacture, presentation and sale of tobacco and related products and repealing Directive 2001/37/EC (Text with EEA relevance)*. 2014, p. 127.

[27] S. Dobaradaran, F. Soleimani, R. Akhbarizadeh, T. C. Schmidt, M. Marzban, et R. BasirianJahromi, « Environmental fate of cigarette butts and their toxicity in aquatic organisms: A comprehensive systematic review », *Environ. Res.*, vol. 195, p. 110881, avr. 2021, doi: 10.1016/j.envres.2021.110881.

[28] T. Luo, Z. Zhang, J. Zhang, C. Sun, et J. I. Yanjun, « Experimental Study on Uniaxial Compressive Strength of Concrete Incorporated with Cigarette Butts », in *IOP Conference Series: Earth and Environmental Science*, IOP Publishing, 2019, p. 052030.

[29] H. Kurmus et A. Mohajerani, « Energy savings, thermal conductivity, micro and macro structural analysis of fired clay bricks incorporating cigarette butts », *Constr. Build. Mater.*, vol. 283, p. 122755, mai 2021.

[30] K. Abdul Kadir et A. Mohajerani, « Effect of heating rate on gas emissions and properties of fired clay bricks and fired clay bricks incorporated with cigarette butts », *Appl. Clay Sci.*, vol. 104, p. 269-276, 28 2015.

[31] A. K. Aeslina et A. Mohajerani, « Leachability of heavy metals from fired clay bricks incorporated with cigarette butts », in *2012 IEEE Symposium on Business, Engineering and Industrial Applications*, IEEE, 2012, p. 872-877.

[32] A. Mohajerani, A. A. Kadir, et L. Larobina, « A practical proposal for solving the world's cigarette butt problem: Recycling in fired clay bricks », *Waste Manag.*, vol. 52, p. 228-244, 01 2016.

[33] M. T. Rahman et A. Mohajerani, « Use of bitumen encapsulated cigarette butts in stone mastic asphalt », *Constr. Build. Mater.*, vol. 261, p. 120530, 20 2020.

[34] M. Morales-Segura, C. Porras-Amores, P. Villoria-Sáez, et D. Caballol-Bartolomé, « Characterization of gypsum composites containing cigarette butt waste for building applications », *Sustainability*, vol. 12, n° 17, p. 7022, 2020.

[35] H. El Fadili, M. Ben Ali, A. el M. Safhi, M. El Mahi, A. Aziz, et E. M. Lotfi, « Effects of encapsulating cellulose acetate microfibers on the mechanical, thermal and environmental properties of geopolymers: A new solution to mitigate the cigarettes pollution », *J. Build. Eng.*, vol. 72, p. 106627, août 2023, doi: 10.1016/j.jobe.2023.106627.

[36] B. Dash, J. Prakash Giri, P. Markandeya Raju, et D. T. K. Dora, « Simultaneous influence of processed cellulose acetate fiber reinforcement and recycled aggregate replacement on mechanical and durability performances of concrete », *Constr. Build. Mater.*, vol. 401, p. 132950, oct. 2023, doi: 10.1016/j.conbuildmat.2023.132950.

[37] J. Tannous, T. Salem, O. Omikrine Metalssi, S. Marceau, et T. Fen-Chong, « Study of the effects of incorporating depolluted cellulose acetate in mortars, with and without superplasticizer, in view of

recycling cigarette butt waste », *Constr. Build. Mater.*, vol. 346, p. 128492, sept. 2022, doi: 10.1016/j.conbuildmat.2022.128492.

[38] K. Xu *et al.*, « Colorful superhydrophobic concrete coating », *Chem. Eng. J.*, vol. 403, p. 126348, janv. 2021, doi: 10.1016/j.cej.2020.126348.

[39] S. Wu, C. Zhang, F. Zhou, S. Ma, et H. Zheng, « The effect of nano-scale calcium stearate emulsion on the integral waterproof performance and chloride resistance of cement mortar », *Constr. Build. Mater.*, vol. 317, p. 125903, janv. 2022, doi: 10.1016/j.conbuildmat.2021.125903.

[40] A. Lagazzo, S. Vicini, C. Cattaneo, et R. Botter, « Effect of fatty acid soap on microstructure of lime-cement mortar », *Constr. Build. Mater.*, vol. 116, p. 384-390, juill. 2016, doi: 10.1016/j.conbuildmat.2016.04.122.

[41] « An alternative admixture to reduce sorptivity of alkali-activated slag cement by optimising pore structure and introducing hydrophobic film - ScienceDirect ». Consulté le: 13 février 2023. [En ligne]. Disponible sur: https://www-sciencedirect-com.univ-eiffel.idm.oclc.org/science/article/pii/S0958946518308679

[42] F. Azarhomayun, M. Haji, M. Kioumarsi, et M. Shekarchi, « Effect of calcium stearate and aluminum powder on free and restrained drying shrinkage, crack characteristic and mechanical properties of concrete », *Cem. Concr. Compos.*, vol. 125, p. 104276, janv. 2022, doi: 10.1016/j.cemconcomp.2021.104276.

[43] L. Falchi, E. Zendri, U. Müller, et P. Fontana, « The influence of water-repellent admixtures on the behaviour and the effectiveness of Portland limestone cement mortars », *Cem. Concr. Compos.*, vol. 59, p. 107-118, mai 2015, doi: 10.1016/j.cemconcomp.2015.02.004.

[44] L. Courard, A. Darimont, M. Schouterden, F. Ferauche, X. Willem, et R. Degeimbre, « Durability of mortars modified with metakaolin », *Cem. Concr. Res.*, vol. 33, n° 9, p. 1473-1479, sept. 2003, doi: 10.1016/S0008-8846(03)00090-5.

[45] R. Harbi, R. Derabla, et Z. Nafa, « Improvement of the properties of a mortar with 5% of kaolin fillers in sand combined with metakaolin, brick waste and glass powder in cement », *Constr. Build. Mater.*, vol. 152, p. 632-641, oct. 2017, doi: 10.1016/j.conbuildmat.2017.07.062.

[46] B. B. Sabir, S. Wild, et J. Bai, « Metakaolin and calcined clays as pozzolans for concrete: a review », *Cem. Concr. Compos.*, vol. 23, n° 6, p. 441-454, déc. 2001, doi: 10.1016/S0958-9465(00)00092-5.

[47] U. Jamilu, M. Usman, I. Abdullahi Getso, et G. Sanusi, « Evaluation of compressive strength of metakaolin-rice husk ash- ternary blended mortar using surface response methodology », *Mater. Today Proc.*, mars 2023, doi: 10.1016/j.matpr.2023.03.120.

[48] M. S. Nawab *et al.*, « A study on improving the performance of cement-based mortar with silica fume, metakaolin, and coconut fibers », *Case Stud. Constr. Mater.*, vol. 19, p. e02480, déc. 2023, doi: 10.1016/j.cscm.2023.e02480.

[49] AFNOR, « Méthodes d'essais des ciments - Partie 1 : détermination des résistances NF EN 196-1 ». Association Française de Normalisation (AFNOR), septembre 2016. [En ligne]. Disponible sur:

https://www.boutique.afnor.org/fr-fr/norme/nf-en-1961/methodes-dessais-des-ciments-partie-1-determination-des-resistances/fa184622/57803

[50] International Standards Organization, « Ciments — Méthodes d'essai — Détermination de la résistance mécanique ISO 679:2009 ». mai 2009. [En ligne]. Disponible sur: https://www.iso.org/fr/standard/45568.html

[51] S. Amziane, F. Collet, M. Lawrence, C. Magniont, V. Picandet, et M. Sonebi, « Recommendation of the RILEM TC 236-BBM: characterisation testing of hemp shiv to determine the initial water content, water absorption, dry density, particle size distribution and thermal conductivity », *Mater. Struct.*, vol. 50, juin 2017.

[52] AFNOR, « Essais pour béton frais - Partie 2 : essai d'affaissement NF EN 12350-2 ». Association Française de Normalisation (AFNOR), juin 2019. [En ligne]. Disponible sur: https://www.boutique.afnor.org/fr-fr/norme/nf-en-123502/essais-pour-beton-frais-partie-2-essai-daffaissement/fa190558/83431

[53] AFNOR, « Liants hydrauliques - Méthodes d'essais des ciments - Détermination du retrait et du gonflement NF P15-433 ». Association Française de Normalisation (AFNOR), juillet 2023. [En ligne]. Disponible sur: https://www.boutique.afnor.org/fr-fr/norme/nf-p15433/liants-hydrauliques-methodes-dessais-des-ciments-determination-du-retrait-e/fa205982/348880

[54] NF, P., « P 18-459Concrete–Testing hardened concrete–Testing porosity and density ». 2010.

[55] T. Salem, M. Fois, O. Omikrine-Metalssi, R. Manuel, et T. Fen-Chong, « Thermal and mechanical performances of cement-based mortars reinforced with vegetable synthetic sponge wastes and silica fume », *Constr. Build. Mater.*, vol. 264, p. 120213, déc. 2020.

[56] A. Yacoub, A. Djerbi, et T. Fen-Chong, « The effect of the drying temperature on water porosity and gas permeability of recycled sand mortar », *Constr. Build. Mater.*, vol. 214, p. 677-684, juill. 2019.

[57] T. Nochaiya, Y. Sekine, S. Choopun, et A. Chaipanich, « Microstructure, characterizations, functionality and compressive strength of cement-based materials using zinc oxide nanoparticles as an additive », *J. Alloys Compd.*, vol. 630, p. 1-10, mai 2015.

[58] Y. Gao, X. Cui, N. Lu, S. Hou, Z. He, et C. Liang, « Effect of recycled powders on the mechanical properties and durability of fully recycled fiber-reinforced mortar », *J. Build. Eng.*, vol. 45, p. 103574, janv. 2022.

[59] A. Maryoto, R. Setijadi, A. Widyaningrum, et S. Waluyo, « Drying Shrinkage of Concrete Containing Calcium Stearate, (Ca(C18H35O2)2), with Ordinary Portland Cement (OPC) as a Binder: Experimental and Modelling Studies », *Molecules*, vol. 25, n° 21, Art. n° 21, janv. 2020, doi: 10.3390/molecules25214880.

[60] A. K. H. Kwan et W. W. S. Fung, « Effects of SP on flowability and cohesiveness of cement-sand mortar », *Constr. Build. Mater.*, vol. 48, p. 1050-1057, nov. 2013, doi: 10.1016/j.conbuildmat.2013.07.065.

[61] Y. Cui, D. Wang, J. Zhao, D. Li, S. Ng, et Y. Rui, « Effect of calcium stearate based foam stabilizer on pore characteristics and thermal conductivity of geopolymer foam material », *J. Build. Eng.*, vol. 20, p. 21-29, nov. 2018, doi: 10.1016/j.jobe.2018.06.002.

[62] M. Cyr, M. Trinh, B. Husson, et G. Casaux-Ginestet, « Effect of cement type on metakaolin efficiency », *Cem. Concr. Res.*, vol. 64, p. 63-72, oct. 2014, doi: 10.1016/j.cemconres.2014.06.007.

[63] A. M. Rashad, « Metakaolin as cementitious material: History, scours, production and composition – A comprehensive overview », *Constr. Build. Mater.*, vol. 41, p. 303-318, avr. 2013, doi: 10.1016/j.conbuildmat.2012.12.001.

[64] N. R. Buenfeld, « Structure and performance of cements, 2nd edition », *Eng. Struct.*, vol. 25, n° 1, p. 127, 2003.

[65] R. Chen, J. Liu, et S. Mu, « Chloride ion penetration resistance and microstructural modification of concrete with the addition of calcium stearate », *Constr. Build. Mater.*, vol. 321, p. 126188, févr. 2022, doi: 10.1016/j.conbuildmat.2021.126188.

[66] P. K. Mehta et P. J. Monteiro, *Concrete: microstructure, properties, and materials*. McGraw-Hill Education, 2014.

[67] M. Nemati Chari, R. Naseroleslami, et M. Shekarchi, « The impact of calcium stearate on characteristics of concrete », *Asian J. Civ. Eng.*, vol. 20, n° 7, p. 1007-1020, nov. 2019, doi: 10.1007/s42107-019-00161-x.

[68] American Concrete Institute (ACI)), « Report on Chemical Admixtures for Concrete », ACI 212.3R-10, 2010.

[69] E. Badogiannis et S. Tsivilis, « Exploitation of poor Greek kaolins: Durability of metakaolin concrete », *Cem. Concr. Compos.*, vol. 31, n° 2, p. 128-133, févr. 2009, doi: 10.1016/j.cemconcomp.2008.11.001.

[70] W. Zhao, Y. Chen, Z. Liu, L. Wang, et X. Li, « Effects of surface-modified coal-bearing metakaolin and graphene oxide on the properties of cement mortar », *Constr. Build. Mater.*, vol. 372, p. 130796, avr. 2023, doi: 10.1016/j.conbuildmat.2023.130796.

[71] R. Cai, Z. Tian, H. Ye, Z. He, et S. Tang, « The role of metakaolin in pore structure evolution of Portland cement pastes revealed by an impedance approach », *Cem. Concr. Compos.*, vol. 119, p. 103999, mai 2021, doi: 10.1016/j.cemconcomp.2021.103999.

[72] R. Martínez-García, M. I. Sánchez de Rojas, P. Jagadesh, F. López-Gayarre, J. M. Morán-del-Pozo, et A. Juan-Valdes, « Effect of pores on the mechanical and durability properties on high strength recycled fine aggregate mortar », *Case Stud. Constr. Mater.*, vol. 16, p. e01050, juin 2022, doi: 10.1016/j.cscm.2022.e01050.

[73] R. Naseroleslami et M. Nemati Chari, « The effects of calcium stearate on mechanical and durability aspects of self-consolidating concretes incorporating silica fume/natural zeolite », *Constr. Build. Mater.*, vol. 225, p. 384-400, nov. 2019, doi: 10.1016/j.conbuildmat.2019.07.144.

[74] W. Zhu, Q. Feng, Q. Luo, X. Bai, K. Chen, et X. Lin, « Effect of a specific PCE superplasticizer on the initial dissolution and early hydration of Portland cement », *J. Build. Eng.*, vol. 46, p. 103786, avr. 2022, doi: 10.1016/j.jobe.2021.103786.

[75] S. Kawashima et S. P. Shah, « Early-age autogenous and drying shrinkage behavior of cellulose fiber-reinforced cementitious materials », *Cem. Concr. Compos.*, vol. 33, n° 2, p. 201-208, févr. 2011, doi: 10.1016/j.cemconcomp.2010.10.018.

[76] A. Messan, P. Ienny, et D. Nectoux, « Free and restrained early-age shrinkage of mortar: Influence of glass fiber, cellulose ether and EVA (ethylene-vinyl acetate) », *Cem. Concr. Compos.*, vol. 33, n° 3, p. 402-410, mars 2011, doi: 10.1016/j.cemconcomp.2010.10.019.

[77] B. Ma, X. Wang, X. Li, et L. Yang, « Influence of superplasticizers on strength and shrinkage cracking of cement mortar under drying conditions », *J. Wuhan Univ. Technol.-Mater Sci Ed*, vol. 22, p. 358-361, juin 2007, doi: 10.1007/s11595-005-2358-6.

[78] X. Q. Qian, S. L. Zhan, et Y. T. Zhu, « Influence of Superplasticizer and Shrinkage-Reducing Admixtures on Early Age Shrinkage of Concrete », *Key Eng. Mater.*, vol. 405-406, p. 166-173, 2009, doi: 10.4028/www.scientific.net/KEM.405-406.166.

[79] J. Zhang *et al.*, « A novel shrinkage-reducing polycarboxylate superplasticizer for cement-based materials: Synthesis, performance and mechanisms », *Constr. Build. Mater.*, vol. 321, p. 126342, févr. 2022, doi: 10.1016/j.conbuildmat.2022.126342.

[80] A. Kronlöf, M. Leivo, et P. Sipari, « Experimental study on the basic phenomena of shrinkage and cracking of fresh mortar », *Cem. Concr. Res.*, vol. 25, n° 8, p. 1747-1754, déc. 1995, doi: 10.1016/0008-8846(95)00170-0.

[81] AFNOR, « Travaux d'enduits de mortiers NF DTU 26.1 ». Association Française de Normalisation (AFNOR), 2008.

[82] AFNOR, « Méthodes d'essai des éléments de maçonnerie - NF EN 772-1+A1 ». Association Française de Normalisation (AFNOR), décembre 2015.

[83] AFNOR, « Méthodes d'essai des éléments de maçonnerie - NF EN 772-13 ». Association Française de Normalisation (AFNOR), janvier 2001.

[84] AFNOR, « Spécifications pour éléments de maçonnerie NF EN 771-1+A1 ». Association Française de Normalisation (AFNOR), octobre 2015.

[85] H. El Fadili *et al.*, « Determination of properties and environmental impact due to the inclusion of cigarette fibers in mortar: a new solution to mitigate the CB pollution », *Environ. Sci. Pollut. Res.*, mars 2023, doi: 10.1007/s11356-023-26491-7.